Efa6 regulates axon growth, branching and maintenance by eliminating off-track microtubules at the cortex

Yue Qu*[,1], Ines Hahn*[,#,1], Meredith Lees[1], Jill Parkin[1], André Voelzmann[1], Karel Dorey[1], Alex Rathbone[2], Claire Friel[2], Viki Allan[1], Pilar Okenve Ramos[3], Natalia Sanchez-Soriano[3], Andreas Prokop[1,#]

1) The University of Manchester, Manchester Academic Health Science Centre, Faculty of Biology, Medicine and Health, School of Biology, Manchester, UK
2) The University of Nottingham, School of Life Sciences, Faculty of Medicine & Health Sciences, Nottingham, UK
3) Department of Cellular and Molecular Physiology, Institute of Translational Medicine, University of Liverpool, Liverpool, United Kingdom

Running title**:** The role of Efa6 in axon maintenance

Key words: *Drosophila*, neurodegeneration, axons, actin, cytoskeleton, microtubules

* authors contributed equally

authors for correspondence:
The University of Manchester
Faculty of Life Sciences
Oxford Road
Manchester M13 9PT
Tel: +44-(0)161-27-51556
Fax: +44-(0)161-27-51505
Andreas.Prokop@manchester.ac.uk
Ines.Hahn@manchester.ac.uk

Abstract

Axons are the enormously long, cable-like neuronal extensions that wire our nervous system. The formation and prolonged maintenance of these delicate structures requires parallel bundles of microtubules (MTs), which form the structural backbones and highways for life-sustaining transport in axons. In ageing and certain axonopathies, axonal MTs lose their bundled appearances forming areas of disorganisation. To understand this deteriorating condition, we use *Drosophila* and study the various mechanisms that promote axonal MT bundle organisation during development and maintenance. Here we report that the membrane-associated protein Efa6 acts as a typical cortical MT collapse factor eliminating MTs approaching the axonal surface. This action provides a quality control mechanism that prevents MT disorganisation during the formation and maintenance of axons by eliminating

MTs accidentally leaving the axon bundle. Furthermore, it is important for the regulation of axonal growth and branch formation in cultured neurons and *in vivo*. Using structure-function analyses, we show that cytoplasmic localisation of a small N-terminal peptide motif alone causes the disappearance of entire MT networks in mouse fibroblasts and loss of whole axons in *Drosophila* primary neurons; its activity becomes meaningful when restricted to the cell plasma membrane via the plekstrin homology domain present in the Efa6 C-terminus. As explained in detail, our data provide a paradigm for the fundamental and relevant role of cortical collapse factors in neurons.

Introduction

Axons are the cable-like neuronal extensions that wire the nervous system. They are typically 0.5-10 µm in diameter, but can be up to a meter long in humans (Debanne et al., 2011; Prokop, 2013a). Usually, these delicate structures have to be maintained for a lifetime, and it is no surprise that axon decay is a prominent neurodegenerative phenomenon (Fang and Bonini, 2012; Wang et al., 2012). Even in health, we gradually lose about half of our axons towards old age (Adalbert and Coleman, 2012; Medana and Esiri, 2003).

The mechanisms regulating the formation, maintenance and decay of axons are little understood. In this study we focus on the continuous parallel bundles of microtubules (MTs) running all along axons which provide their structural backbones and act as highways for life-sustaining cargo transport between cell bodies and synaptic endings (Prokop, 2013a). Axon swellings with disorganised MTs that have lost their bundled arrangements are believed to be a sign of axon decay (Adalbert and Coleman, 2012). They can be observed in ageing brains (Fiala et al., 2007) and have so far been reported for at least two mouse models of neurodegeneration: spastic paraplegia (SPG4; Online Mendelian Inheritance in Man®/OMIM reference #182601) and hereditary sensory and autonomic neuropathy (HSAN type VI; #614653) (Bernier and Kothary, 1998; Dalpe et al., 1998; Fassier et al., 2013; Fiala et al., 2007; Tarrade et al., 2006). But the mechanisms underlying the formation, maintenance and decay of axonal MT bundles are poorly understood. For example in HSAN VI, axonal swellings with severe MT disorganisation are a pathological hallmark which is caused by functional deficiency of dystonin/BPAG1, a member of the spectraplakin family of microtubule-actin cross-linkers (Bernier and Kothary, 1998; Dalpe et al., 1998); however, it has remained elusive so far how loss of dystonin causes this phenotype (Ferrier et al., 2013).

To overcome such knowledge gaps, we study spectraplakins and other actin/microtubule-binding proteins not in isolation but as part of cellular networks or machinery regulating cytoskeletal dynamics; this is possible in the fruit fly *Drosophila melanogaster* capitalising on its highly amenable genetics (Prokop et al., 2013). This approach led us to propose the model of "local axon homeostasis". It assumes that the axon is a high-force environment that, by default, would lead to MT disorganisation and requires therefore a number of regulatory mechanisms that actively tame MTs into bundles (Prokop, 2016; Voelzmann et al., 2016a). A key factor contributing to this taming process is the dystonin homologue Short stop (Shot); like dystonin mutations, also Shot deficiency causes severe disorganisation of axonal MTs (Sánchez-Soriano et al., 2009); capitalising on its experimental amenability in the fly, we were able to identify a number of underlying candidate mechanisms which can now serve as helpful paradigms for work on mammalian spectraplakins (Voelzmann et al., 2017). So far best understood is a guidance mechanism where Shot simultaneously binds to cortical actin via its N-terminus, and to the tips of polymerising MTs through its C-terminus, thus guiding extending MTs in parallel to the axonal cortex and laying

them out into bundles (Alves-Silva et al., 2012).

In the absence of Shot function, MTs leave their bundled arrangements and go off-track, and they also display a drastic decrease in the lifetime of their polymerisation events (Alves-Silva et al., 2012). We therefore hypothesised that off-track MTs might be actively eliminated in axons - for example through the action of proteins at the axonal surface that capture and disassemble MTs (also called cortical MT collapse factors). Various candidates for cortical collapse factors are suggested by the literature: (1) The *Drosophila* katanin Kat60 was shown to localise cortically to regulate cell migration (Zhang et al., 2011). (2) Mutations in the cortically anchored and MT-destabilising kinesin-4 family member KIF21A cause the eye movement disorder 'congenital fibrosis of extraocular muscles' (OMIM reference #135700) (Tiab et al., 2004) and were shown to influence axonal growth and branch formation in mammalian hippocampal neurons (van der Vaart et al., 2013). (3) The *C. elegans* protein Exchange factor for Arf6 (*Ce*Efa6) was reported to act as a cortical collapse factor in oocytes (O'Rourke et al., 2010), and is strongly expressed in neurons where it negatively regulates axon growth and regeneration (Chen et al., 2015; Chen et al., 2011; Eva et al., 2017). However, so far it has remained unclear how these factors regulate neuronal morphology.

Here we focussed on *Drosophila* Efa6. We show that it acts as a cortical collapse factor in mouse fibroblasts and in fly neuron, where it is essential for axonal MT bundle maintenance, growth and branching - both in cultured neurons and in the adult fly brain *in vivo*. The morphological phenotypes we demonstrate are consistent with findings for the other collapse factors, but provide the necessary subcellular understanding to explain how the molecular mechanism of cortical collapse leads to the observed morphological changes in neurons.

Methods

Fly stocks

Loss-of-function mutant stocks used in this study were the two deficiencies uncovering the *Efa6* locus *Df(3R)Exel6273* (94B2-94B11 or 3R:22,530,780..22,530,780) and *Df(3R)ED6091i* (94B5-94C4 or 3R:22,587,681..22,587,681), $shot^{3}$ (the strongest available allele of *short stop*) (Kolodziej et al., 1995; Sánchez-Soriano et al., 2009), and the null mutant alleles $Efa6^{KO\#1}$, $Efa6^{GX6[w-]}$, $Efa6^{GX6[w+]}$ and $Arf51F^{GX16[w-]}$ (all genomically engineered precise deletions) (Huang et al., 2009). Gal4 driver lines used were the pan-neuronal lines *sca-Gal4* (strongest in embryos) (Sánchez-Soriano et al., 2010a) and *elav-Gal4* (1st and 3rd chromosomal, both expressing at all stages) (Luo et al., 1994), as well as the *ato-Gal4* line expressing in a subset of neurons in the adult brain (Hassan et al., 2000; Voelzmann et al., 2016b) and *GMR31F10-Gal4* (Bloomington #49685) expressing in a subset of lamina neurons. Lines for targeted gene expression were $UAS\text{-}Efa6^{RNAi}$ (VDRC #42321), $UAS\text{-}Gal80^{ts}$ (Zeidler et al., 2004), *UAS-Eb1-GFP* (Alves-Silva et al., 2012), *UAS-α-tubulin84B* (Grieder et al., 2000) and *UAS-tdTomato* (Zschätzsch et al., 2014). Efa6 expression was detected via the genomically engineered *Efa6-GFP* allele, where a GFP was inserted after the last amino acid in exon 14 (Huang et al., 2009).

Drosophila primary cell culture

Drosophila primary neuron cultures were performed as published previously (Prokop et al., 2012; Qu et al., 2017). In brief, stage 11 embryos were treated for 1 min with bleach to

remove the chorion, sterilized for ~30 s in 70% ethanol, washed in sterile Schneider's/FCS, and eventually homogenized with micro-pestles in 1.5 centrifuge tubes containing 21 embryos per 100 µl dispersion medium (Prokop et al., 2012) and left to incubated for 5 min at 37°C. Cells are washed with Schneider's medium (Gibco), spun down for 4 mins at 650 g, supernatant was removed and cells re-suspended in 90 µl of Schneider's medium containing 20% fetal calf serum (Gibco). 30 µl drops were placed on cover slips. Cells were allowed to adhere for 90-120 min either directly on glass or on cover slips coated with a 5 µg/ml solution of concanavalin A, and then grown as a hanging drop culture for hours or days at 26°C as indicated.

For the transfection of *Drosophila* primary neurons, a quantity of 70-75 embryos per 100 µl dispersion medium was used. After the washing step and centrifugation, cells were re-suspended in 100 µl transfection medium [final media containing 0.1-0.5 µg DNA and 2 µl Lipofecatmine 2000 (L2000)]. To generate this media, dilutions of 0.1-0.5 µg DNA in 50 µl Schneider's medium and 2 µl L2000 in 50 µl Schneider's medium were prepared, then mixed together and incubated at room temperature for 5-30 mins, before being added to the cells in centrifuge tubes where they were kept for 24 hrs at 26°C. Cells were then treated again with dispersion medium, re-suspended in culture medium and plated out as described above.

For temporally controlled knock-down experiments we used flies carrying the driver construct *elav-Gal4*, the knock-down construct *UAS-Efa6-RNAi*, and the temperature-sensitive Gal4 inhibitor *UAS-Gal80^{ts}*, all in parallel. At the restrictive temperature of 19°C, Gal80^{ts} blocks Gal4-induced expression of *Efa6-RNAi*, and this repressive action is removed at the permissive temperature of 27°C where Gal80^{ts} is non-functional. Control neurons were from flies carrying only the *Gal4/Gal80* or the *Efa6-RNAi* transgene.

<u>Fibroblast cell culture</u>

NIH/3T3 fibroblasts were grown in DMEM supplemented with 1% glutamine (Invitrogen), 1% penicillin/streptomycin (Invitrogen) and 10% FCS in culture dishes (100 mm with vents; Fisher Scientific UK Ltd) at 37°C in a humidified incubator at 5% CO_2. Cells were split every 2-3 d, washed with pre-warmed PBS, incubated with 4 ml of Trypsin-EDTA (T-E) at 37°C for 5 min, then suspended in 7 ml of fresh culture medium and eventually diluted (1/3-1/20 dilution) in a culture dish containing 10 ml culture media.

For transfection of NIH/3T3 cells, 2 ml cell solution (~10^5 cells per ml) were first transferred to 6-well plates, and grown overnight to double cell density. 2 µg of DNA and 2 µl Plus reagent (Invitrogen) were added to 1 ml serum-free media in a centrifuge tube, incubated for 5 mins at RT, then 6 µl Lipofectamine (Invitrogen) were added, and incubated at RT for 25 mins. Cells in the 6-well plate were washed with serum-free medium and 25 mins later DNA/Lipofectamine was mixed into the medium (1/1 dilution). Plates were incubated for 3 hrs at 37°C, washed with 2 ml PBS, 400 µl trypsin were added for 5 mins (37°C), then 3 ml complete medium; cells were suspended and added in 1 ml aliquots to 35 mm glass-bottom dishes (MatTek) coated with fibronectin [300 µl of 5 µg/ml fibronectin (Sigma-Aldrich) placed in the center of a MatTek dish for 1 hr at 37°C, then washed with PBS]; 1 ml of medium was added and cells grown for 6 hrs or 24 hrs at 37°C in a CO_2 incubator. For live imaging, the medium was replaced with 2 ml Ham's F-12 medium + 4% FCS.

<u>Dissection of adult heads</u>

To analyse the function of Efa6 in MT bundle integrity in medulla axons *in vivo*, flies were aged at 29°C. Flies were maintain in groups of up to 20 flies of the same gender (Stefana et al., 2017) and changed into new tubes every 3-4 days. Brain dissections were performed in Dulbecco's PBS (Sigma, RNBF2227) after briefly sedating them on ice. Dissected brains with their laminas and eyes attached were placed into a drop of Dulbecco's PBS on MatTek glass bottom dishes (P35G1.5-14C), covered by coverslips and immediately imaged with a 3i Marianas Spinning Disk Confocal Microscope.

To measure branching in *ato-Gal4 Drosophila* neurons, adult brains were dissected in Dulbecco's PBS and fixed with 4% PFA for 15 min. Antibody staining and washes were performed with PBS supplemented with 0.3% Triton X-100. Specimens were embedded in Vectashield (VectorLabs).

Immunohistochemistry

Primary fly neurons and fibroblasts were fixed in 4% paraformaldehyde (PFA) in 0.05 M phosphate buffer (PB; pH 7–7.2) for 30 min at room temperature (RT); for anti-Eb1 staining, ice-cold +TIP fix (90% methanol, 3% formaldehyde, 5 mM sodium carbonate, pH 9; stored at -80°C and added to the cells) (Rogers et al., 2002) was added for 10 mins. Adult brains were dissected out of their head case in PBS and fixed with 4% PFA in PBS for 1 hr, followed by a 1hr wash in PBT.

Antibody staining and washes were performed with PBT. Staining reagents: anti-tubulin (clone DM1A, mouse, 1:1000, Sigma; alternatively, clone YL1/2, rat, 1:500, Millipore Bioscience Research Reagents); anti-DmEb1 (gift from H. Ohkura; rabbit, 1:2000) (Elliott et al., 2005); anti-Elav (mouse, 1:1000, DHB); anti-GFP (goat, 1:500, Abcam); Cy3-conjugated anti-HRP (goat, 1:100, Jackson ImmunoResearch); F-actin was stained with Phalloidin conjugated with TRITC/Alexa647, FITC or Atto647N (1:100 or 1:500; Invitrogen and Sigma). Specimens were embedded in ProLong Gold Antifade Mountant.

Microscopy and data analysis

Standard documentation was performed with AxioCam monochrome digital cameras (Carl Zeiss Ltd.) mounted on BX50WI or BX51 Olympus compound fluorescent microscopes. For the analysis of *Drosophila* primary neurons, we used two well established parameters (Alves-Silva et al., 2012; Sánchez-Soriano et al., 2010a): axon length (from cell body to growth cone tip; measured using the segmented line tool of ImageJ) and the degree of MT disorganisation in axons which was either measured as binary score or ratio (percentage of neurons showing obvious MT disorganisation in their axons) or as "MT disorganisation index" (MDI) (Qu et al., 2017): the area of disorganisation was measured using the freehand selection in ImageJ; this value was then divided by axon length (see above) multiplied by 0.5 µm (typical axon diameter, thus approximating the expected area of the axon if it were not disorganised). For Eb1::GFP comet counts, neurons were subdivided into axon shaft and growth cones (GC): the proximal GC border was set where the axon widens up (broader GCs) or where filopodia density increases significantly (narrow GCs). MT loss in fibroblasts was assessed on randomly chosen images of successfully transfected, GFP-expressing fibroblasts, stained for tubulin and actin. Images were derived from at least 2 independent experimental repeats performed on different days, for each of which at least 3 independent culture wells were analysed by taking a minimum of 20 images per well. Due to major differences in plasma

membrane versus cytoplasmic localisation of constructs, their expression strengths could not be standardised. Assuming a comparable expression strength distribution, we therefore analyse all transfected cells in the images and assigned them to three categories: MTs intact, damaged or gone (Fig. 8). To avoid bias, image analyses were performed blindly, i.e. the genotype or treatment of specimens was masked. To analyse ruffle formation in fibroblasts, cells were stained with actin and classified (with or without ruffles).

To measure the degree of branching in *ato-Gal4* neurons, Z-stacks of adult fly brains (optic lobe area) were taken with a Leica DM6000 B microscope and extracted with Leica MM AF Premier software. They were imaged from anterior and the number of branches was quantified manually. Branches were defined as the protrusions from the DC neuron axons in the medulla. Branches in fly primary neurons at 5DIV were also counted manually and defined as MT protrusions from main axon.

To measure MT disorganisation in the optic lobe of adult flies, *GMR31F10-Gal4* (Bloomington #49685) was used to express *UAS-α-tubulin84B-GFP* (Grieder et al., 2000) in a subset of lamina axons which projects within well-ordered medulla columns. A section of the medulla columns comprising the 4 most proximal axonal terminals was used to quantify the number of swellings and regions with disorganised MTs.

Time lapse imaging of cultured primary neurons (in Schneider's/FCS) and fibroblasts (in Ham's F-12/FCS) was performed on a Delta Vision Core (Applied Precision) restoration microscope using a [*100x/1.40 UPlan SAPO (Oil)*] objective and the Sedat Quad filter set (*Chroma #89000*). Images were collected using a Coolsnap HQ2 (Photometrics) camera. The temperature was set to 26°C for fly neurons and 37°C for fibroblasts. Time lapse movies were constructed from images taken every 2 s for 2 mins. To analyse MT dynamics, Eb1::GFP comets were tracked manually using the "manual tracking" plug-in of ImageJ.

For statistical analyses, Kruskal–Wallis one-way ANOVA with *post hoc* Dunn's test or Mann–Whitney Rank Sum Tests (indicated as P_{MW}) were used to compare groups, and $\chi 2$ tests (indicated as P_{X2}) were used to compare percentages. All raw data of our analyses are provided as supplementary Excel/Prism files.

<u>Molecular biology</u>

EGFP tags are based on pcDNA3-EGFP or pUAST-EGFP. All *Drosophila melanogaster* efa6 constructs are based on cDNA cloneIP15395 (Uniprot isoform C, intron removed). *Caenorhabditis elegans* efa-6 (Y55D9A.1a) constructs are derived from pCZGY1125-efa-6-pcr8 (kindly provided by Andrew Chisholm). *Homo sapiens* PSD(1) (ENST00000406432.5, isoform 202) constructs were PCR-amplified from pLC32-hu-psd1-pcr8 vector (kindly provided by Andrew Chisholm). *Homo sapiens* PSD2 (ENST00000274710.3, isoform 201, 771aa) constructs were PCR-amplified from pLC33-hu-psd2-pcr8 vector (kindly provided by Andrew Chisholm). *Homo sapiens* PSD3 was PCR-amplified from pLC34 hu-psd3-pcr8 vector (kindly provided Andrew Chisholm). Note that the PSD3 cDNA clone is most closely related to isoform 201 (ENST00000286485.12: 513aa) and therefore lacks the putative N-terminus found in isoform 202 (ENST00000327040.12). However, the putative MTED core sequence is encoded in the C-terminal PH domain (Fig.8C), not the potential N-terminus. *Homo sapiens* PSD4 (ENST00000441564.7, isoform 205) was PCR-amplified from pLC35-hu-psd4-pcr8 vector (kindly provided by Andrew Chisholm).The CAAX motif is derived from human KRAS. The *Dm*Efa6-NterminΔSxiP::EGFP (aa1-410) insert was synthesised by GeneArt Express (ThermoFisher). All construct were cloned using standard (SOE) PCR/ligation based methods, and constructs and

inserts are detailed in Table T1. To generate transgenic fly lines, *P[acman]M-6-attB-UAS-1-3-4* constructs were integrated into *PBac{yellow[+]-attP-3B}VK00031* (Bloomington line #9748) via PhiC31 mediated recombination (outsourced to Bestgene Inc.).

final vector	**Source**	**insert**
pcDNA3-EGFP	Addgene	*XhoI*-EGFP-*XbaI*
pUAST-AscI-PacI-EGFP	this study	*KpnI, AscI, PacI*-EGFP-*XbaI*
pUAST-*Dm*Efa6FL::EGFP (aa1-1387)	this study	*KpnI, AscI*-***kozak***-Efa6 (aa1-1387)-**GSGSGS-EGFP**-*PacI, XbaI*
P[acman]M-6-attB-UAS-1-3-4-*Dm*Efa6FL::EGFP (aa1-1387)	this study	*AscI*-***kozak***-*Dm*Efa6 (aa1-1387)-**GSGSGS-EGFP**-*PacI*
pcDNA3.1-*Dm*Efa6FL::EGFP (aa1-1387)	this study	*KpnI, AscI*-***kozak***-*Dm*Efa6 (aa1-1387)-**GSGSGS-EGFP**-*PacI, XbaI*
pUAST-*Dm*Efa6ΔCterm::EGFP (aa1-894)	this study	*KpnI, AscI*-***kozak***-*Dm*Efa6Δ**Cterm** (aa1-894)-**GSGSGS-EGFP**-*PacI, XbaI*
P[acman]M-6-attB-UAS-1-3-4-*Dm*Efa6ΔCterm::EGFP (aa1-894)	this study	*AscI*-***kozak***-*Dm*Efa6Δ**Cterm** (aa1-894)-**GSGSGS-EGFP**-*PacI*
pcDNA3.1-*Dm*Efa6ΔCterm::EGFP (aa1-894)	this study	*KpnI, AscI*-***kozak***-*Dm*Efa6Δ**Cterm** (aa1-894)-**GSGSGS-EGFP**-*PacI, XbaI*
pUAST-*Dm*Efa6-Nterm::EGFP (aa1-410)	this study	*KpnI, AscI*-***kozak***-*Dm*Efa6-Nterm (aa1-410)-**GSGSGS-EGFP**-*PacI, XbaI*
P[acman]M-6-attB-UAS-1-3-4-*Dm*Efa6-Nterm::EGFP (aa1-410)	this study	*AscI*-***kozak***-*Dm*Efa6-Nterm (aa1-410)-**GSGSGS-EGFP**-*PacI*
pcDNA3.1-*Dm*Efa6-Nterm::EGFP (aa1-410)	this study	*KpnI, AscI*-***kozak***-*Dm*Efa6-Nterm (aa1-410)-**GSGSGS-EGFP**-*PacI, XbaI*
pUAST-*Dm*Efa6-Nterm-CAAX::EGFP (aa1-410)	this study	*KpnI, AscI*-***kozak***-*Dm*Efa6-Nterm (aa1-410)-**GSGSGS-EGFP-CAAX[KRAS]**-*PacI, XbaI*
P[acman]M-6-attB-UAS-1-3-4-*Dm*Efa6-Nterm-CAAX::EGFP (aa1-410)	this study	*AscI*-***kozak***-*Dm*Efa6-Nterm (aa1-410)-**GSGSGS-EGFP-CAAX[KRAS]**-*PacI*
pcDNA3.1-*Dm*Efa6-Nterm-CAAX::EGFP (aa1-410)	this study	*KpnI, AscI*-***kozak***-*Dm*Efa6-Nterm (aa1-410)-**GSGSGS-EGFP-CAAX[KRAS]**-*PacI, XbaI*
pUAST-*Dm*Efa6-NtermΔSxiP::EGFP (aa1-410)	this study	*KpnI, AscI*-***kozak***-*Dm*Efa6-NtermΔ**SxiP** (aa1-410; **SQIP>AAAA; SRIP>AAAA**)-**GSGSGS-EGFP**-*PacI, XbaI*
pcDNA3.1-*Dm*Efa6-NtermΔSxiP::EGFP (aa1-410)	this study	*KpnI, AscI*-***kozak***-*Dm*Efa6-NtermΔ**SxiP** (aa1-410; **SQIP>AAAA; SRIP>AAAA**)-**GSGSGS-EGFP**-*PacI, XbaI*
pUAST-*Dm*Efa6-NtermΔMTED::EGFP (aa1-300)	this study	*KpnI, AscI*-***kozak***-*Dm*Efa6-NtermΔ**MTED** (aa1-300)-**GSGSGS-EGFP**-*PacI, XbaI*
pcDNA3.1-*Dm*Efa6-NtermΔMTED::EGFP (aa1-300)	this study	*KpnI, AscI*-***kozak***-*Dm*Efa6-NtermΔ**MTED** (aa1-300)-**GSGSGS-EGFP**-*PacI, XbaI*
pUAST-*Dm*Efa6ΔNerm::EGFP (aa851-1387)	this study	*KpnI, AscI*-***kozak***-*Dm*Efa6Δ**Nerm** (aa851-1387)-**GSGSGS-EGFP**-*PacI, XbaI*
pcDNA3.1-*Dm*Efa6ΔNerm::EGFP (aa851-1387)	this study	*KpnI, AscI*-***kozak***-*Dm*Efa6Δ**Nerm** (aa851-1387)-**GSGSGS-EGFP**-*PacI, XbaI*
pUAST-*Dm*Efa6-MTED::EGFP (aa322-341)	this study	*KpnI, AscI*-***kozak***-*Dm*Efa6-MTED (aa322-341)-**GSGSGS-EGFP**-*PacI, XbaI*
pcDNA3.1-*Dm*Efa6-MTED::EGFP (aa322-341)	this study	*KpnI, AscI*-***kozak***-*Dm*Efa6-MTED (aa322-341)-**GSGSGS-EGFP**-*PacI, XbaI*
pcDNA3.1-*Ce*Efa6-FL::EGFP (aa1-816)	this study	*KpnI, AscI*-***kozak***-*Ce*Efa6 (aa1-816)-**GSGSGS-EGFP**-*PacI, XbaI*
pcDNA3.1-*Ce*Efa6-Nterm::EGFP (aa1-152)	this study	*KpnI, AscI*-***kozak***-*Ce*Efa6-Nterm (aa1-152)-**GSGSGS-EGFP**-*PacI, XbaI*
pcDNA3.1-*Ce*Efa6-MTED::EGFP (aa24-42)	this study	*KpnI, AscI*-***kozak***-*Ce*Efa6-MTED (aa24-42)-**GSGSGS-EGFP**-*PacI, XbaI*

pcDNA3.1-*Hs*PSD(1)-FL::EGFP (aa1-1024)	this study	*KpnI, AscI*-***kozak***-*Hs*PSD(1) (aa1-1024)-**GSGSGS-***NotI*-**EGFP**-*PacI, XbaI*
pcDNA3.1-*Hs*PSD(1)-Nterm::EGFP (aa1-280)	this study	*KpnI, AscI*-***kozak***-*Hs*PSD(1)-Nterm (aa1-280)-**GSGSGS**-*NotI*-**EGFP**-*PacI, XbaI*
pcDNA3.1-*Hs*PSD(1)-MTED::EGFP (aa31-49)	this study	*KpnI, AscI*-***kozak***-*Hs*PSD(1)-MTED (aa31-49)-**GSGSGS**-*NotI*-**EGFP**-*PacI, XbaI*
pcDNA3.1-*Hs*PSD2-FL::EGFP (aa1-771)	this study	*KpnI, AscI*-***kozak***-*Hs*PSD2 (aa1-771)-**GSGSGS**-*NotI*-**EGFP**-*PacI, XbaI*
pcDNA3.1-*Hs*PSD3::EGFP (aa515-1047)	this study	*KpnI, AscI*-***kozak***-*Hs*PSD3 (aa515-1047)-**GSGSGS**-*NotI*-**EGFP**-*PacI, XbaI*
pcDNA3.1-*Hs*PSD4-FL::EGFP (aa1-1027)	this study	*KpnI, AscI*-***kozak***-*Hs*PSD4 (aa1-1027)-**GSGSGS-***NotI*-**EGFP**-*PacI, XbaI*
pcDNA3.1-co-*Hs*PSD(1)-MTED::EGFP (aa31-49)	this study	*KpnI, AscI*-***kozak***-*Hs*PSD(1)-MTED (aa31-49)-**GSGSGS-EGFP**-*PacI, XbaI*
pcDNA3.1-co-*Ce*Efa6-MTED::EGFP (aa24-42)	this study	*KpnI, AscI*-***kozak***-*Ce*Efa6-MTED (aa24-42)-**GSGSGS-EGFP**-*PacI, XbaI*
pcDNA3.1-co-*Dm*Efa6-MTED::EGFP (aa322-341)	this study	*KpnI, AscI*-***kozak***-*Dm*Efa6-MTED (aa322-341)-**GSGSGS-EGFP**-*PacI, XbaI*
pCS107-*Dm*Efa6-Nterm::EGFP	this study	*NotI*-***kozak***-*Dm*Efa6-Nterm (aa1-410)-***GSGSGS-EGFP***-*StuI*
RFP (*Xenopus* injection)	tba	tba
pFastBac-His6-MCAK::EGFP-StrepII	tba	His6-MCAK::EGFP-StrepII
pFastBac-His6-*Dm*Efa6ΔCterm::EGFP-StrepII (aa1-894)	this study	His6-*Dm*Efa6Δ**Cterm**::EGFP-StrepII (aa1-894)

Tab. T1. co=codon optimised; *Dm=Drosphila melanogaster*; *Ce=Caenorhabditis elegans*; *Hs=Homo sapiens*

In silico analyses

To generate the **phylogenetic tree** of Efa6/PSD full length isoforms and N-terms of different species (see Fig. S3), their amino acid sequences were aligned using Muscle or ClustalO (Goujon et al., 2010; McWilliam et al., 2013; Sievers et al., 2011). ProtTest (Abascal et al., 2005; Darriba et al., 2011) was used to determine amino acid frequencies in the protein datasets and to identify the optimal amino acid substitution model to be used for the Bayesian inference (VT+I+G+F). CUDA-Beagle-optimised MrBayes (Ronquist et al., 2012) was run using the VT+I+G+F model [prset statefreqpr=fixed(empirical); lset rates=invgamma] using 5 chains (1 heated) and 9 parallel runs until the runs converged and standard deviation of split frequencies were below 0.015 (0.06 for N-terms); PSRF+ was 1.000 and min ESS was >1300 for the TL, alpha and pinvar parameters. The *Drosophila melanogaster* Sec7-PH domain-containing protein Steppke was used as outgroup in the full length tree. Archaeopteryx (Han and Zmasek, 2009) was used to depict the MrBayes consensus tree showing branch lengths (amino acid substitutions per site) and Bayesian posterior probabilities.

To **identify a potential MTED in PSD(1)**, previously identified Efa6 MTED motifs (O'Rourke et al., 2010) of 18 orthologues were aligned to derive an amino acid logo (T10). Further orthologues were identified and used to refine the logo. Invariant sites and sites with restricted amino acid substitutions were determined (most prominently MxG-stretch). Stretches containing the invariant MxG stretch were aligned among vertebrate species to identify potential candidates. Berkley's Weblogo server (Crooks et al., 2004) was used to generate amino acid sequence logos for each phylum using MTED (ExxxMxGE/D) and MTED-like (MxGE/D) amino acid stretches.

In vitro analyses

Protein Expression and Purification: *Drosophila* Efa6-ΔCterm was cloned into a modified pFastBac vector containing an N-terminal *His6* tag and C-terminal *eGFP* and *StrepII* tags. Recombinant protein was expressed in Sf9 insect cells for 72 hours using a Baculovirus system. The protein was purified via a two-step protocol. Cleared lysate was loaded onto a 1ml HisTrap column (GE Healthcare) in Ni-Affinity buffer [50 mM Tris pH 7.5, 300 mM NaCl, 10 % (v/v) glycerol, 1 mMM was shipped as lyophilized powder with a purity of 95.2%. Upon arrival peptide was dissolved in ultrapure water and stored at -20°C.

MT binding assays: GMPCPP-stabilised, rhodamine-labeled MTs were adhered to the surface of flow chambers as described earlier (Helenius et al., 2006). 20 nM Efa6-ΔCterm::GFP (in BRB20 pH 6.9, 75mM KCl, 0.05% Tween20, 0.1 mg/ml BSA, 1% 2-mercaptoethanol, 40mM glucose, 40 mg/ml glucose oxidase, 16 mg/ml catalase), 20 nM MCAK::GFP (in the same buffer plus 1 mM ATP and 1 mM taxol) was introduced to the MT-containing channel. Images were recorded using a Zeiss Observer.Z1 microscope equipped with a Zeiss Laser TIRF 3 module, QuantEM 512SC EMCDD camera (Photometrics) and 100x objective (Zeiss, alphaPlanApo/1.46NA oil). Images of rhodamine-labeled MTs using a lamp as the excitation source and GFP fluorescence using TIRF illumination via a 488 nm laser were collected as described earlier (Patel et al., 2016). For both rhodamine and GFP imaging an exposure time of 100 ms was used. The mean GFP intensity on individual MTs was determined from the mean pixel intensity of lines drawn along the long-axis of individual microtubules in Fiji (Schindelin et al., 2012). The rhodamine signal was used to locate the position of MTs in the GFP images. Intensity from a region of background was subtracted.

MT depolymerisation assays: Single-cycled, rhodamine-labeled, GMPCPP-stabilised MTs were adhered to the surface of flow chambers as described in (Helenius et al., 2006). Images of a field of fluorescent microtubules (25% rhodamine-labeled tubulin) were recorded using a Zeiss Observer.Z1 microscope, collecting 1 image every 5 s with an exposure time of 100 ms. Efa6-ΔCterm::GFP (14 nM), MCAK (40 nM) in solution (BRB20 pH 6.9, 75mM KCl, 1mM ATP, 0.05% Tween 20, 0.1 mg/ml BSA, 1% 2-mercaptoethanol, 40mM glucose, 40 mg/ml glucose oxidase, 16 mg/ml catalase) were added to the channel 1 min after acquisition had commenced. De-polymerisation rates were determined from plots of the length of individual microtubules versus time, obtained by thresholding and particle analysis of images using Fiji (Schindelin et al., 2012).

***Xenopus* oocyte assays**: cytosol extracts from *Xenopus* oocytes were obtained as described in (Allan and Vale, 1991). **MT depolymerisation** was assessed in a microscopic flow chamber (Vale and Toyoshima, 1988) where *Xenopus* cytosol (1 µl cytosol diluted with 20 µl acetate buffer) was incubated for 20 min to allow MTs to polymerise. Then cytosol was exchanged by flow through with Efa6-ΔCterm::GFP, MCAK or synthetic MTED peptide (all 20 nM in acetate buffer pH 7.4: 100 mM K-Acetate, 3 mM Mg-Acetate, 5 mM EGTA, 10 mM HEPES), and MT length changes observed by recording 10 random fields via VE-DIC microscopy (Allan, 1993; Allan and Vale, 1991). **MT polymerisation** was analysed in a microscope flow cell containing 9 µl diluted *Xenopus* cytosol (see above) to which 1 µl acetate buffer was added, either alone or containing 20nM MTED. After 10 min, 20 random fields were recorded via VE-DIC microscopy for each condition and the numbers of MTs per field counted.

For the *in vivo* assay, *Xenopus* embryos were injected in one blastomere at the 4-cell stage

with 200 ng of mRNA encoding Efa6-Nterm::GFP or mCherry alone. The embryos were imaged at stage 10.25 (Heasman, 2006) with a Leica fluorescent stereoscope.

Results

Efa6 is a negative regulator of axonal growth and branching in cultured neurons and *in vivo*

We wanted to establish whether Efa6 may act as a regulator of axonal MT networks required for the growth, maintenance and morphology of *Drosophila* neurons. We first established whether and where it might be expressed in the nervous system. For this, we used a genomically engineered GFP-tagged version of the endogenous *Efa6* gene (*Efa6-GFP*) that was previously shown to be expressed in the embryonic CNS (Huang et al., 2009). Using the same *Efa6-GFP* line, we found that Efa6 continues to be expressed throughout the CNS at larval and adult stages, likely to be present in most or even all neurons (Fig. 1F-I). To determine the subcellular localisation, analyses in primary neurons obtained from the *Efa6-GFP* line analysed after 6 hrs *in vitro* (HIV) and at 5 days *in vitro* (DIV), revealed reliable expression of GFP in cell bodies and all along their axons (Fig. 1A-E). We then studied whether Efa6 is important for axonal morphogenesis by decreasing or enhancing its function. We found robust effects on axon growth and collateral branching.

For this, we first analysed primary fly neurons with loss of Efa6 function at 6 hrs *in vitro* (6HIV; Fig. 2A-D) using a number of conditions: Efa6 knock-down (*Efa6-RNAi*), overlapping deficiencies uncovering the entire *Efa6* gene locus ($Efa6^{Def}$), or different loss-of-function mutant alleles generated by genomic engineering ($Efa6^{KO\#1}$, $Efa6^{GX6[w-]}$, $Efa6^{GX6[w+]}$). In all these cases, axon length was robustly increased up to over 120% when compared to wild-type controls. We also generated transgenic fly lines for the targeted expression of Efa6-FL::GFP. When expressing it in primary neurons using the pan-neuronal driver line *sca-Gal4*, we found a reduction to ~80% (all normalised to wild-type controls; Figs. 2C,D). Together these results suggested Efa6 to exhibit a growth inhibiting role.

We then assessed collateral branching, focussing on mature primary neurons at 5 days *in vitro* (DIV). We found that $Efa6^{KO\#1}$ homozygous mutant neurons showed an increase in collateral branches to 193% ±14SEM (Fig.2F,I). *Vice versa*, neurons expressing Efa6-FL::GFP showed a reduction in side branches at 5 DIV to 79% ± 4SEM (Fig.2G,I). To extend these studies to neurons *in vivo*, we measured axonal projections of dorsal cluster neurons in the medulla, which is part of the optic lobe in the adult brain (Fig.3) (Hassan et al., 2000; Voelzmann et al., 2016b). These neurons were labelled by expressing *UAS-myr-tdTomato* via the *ato-Gal4* driver either alone (control), together with $UAS\text{-}Efa6^{RNAi}$ or together with *UAS-Efa6-FL-GFP*. We analysed them in young brains (2-5 d after eclosure of flies from their pupal case) or old brains (15-18 d; Figs.3, S1). When comparing control to experimental brains, we found that *Efa6* knock-down in dorsal cluster neurons caused a significant increase in branch numbers to 129% ± 4SEM at young and to 138% ± 4SEM at old stages. In contrast, whereas over-expression of Efa6::GFP strongly decreased branch numbers to 67% ± 4SEM at young and 72% ± 2SEM at old stages (Fig.3G).

In these experiments, Efa6-FL::GFP had an intriguing further effect, in that only 57% of young brains had any axon protrusion in the medulla region, compared to 88% in controls (Figs.3C,H, S1B). Because axons are eventually present in the old brains (91% control and 89% Efa6-FL; Fig.3F,H, S1D), this phenotype reflects delayed outgrowth and likely is the *in*

vivo equivalent to short axon growth observed upon Efa6 over-expression in primary neurons (green bars in Fig.2D).

These data obtained from neurons in culture and in the adult brain, clearly demonstrate that the presence of Efa6 in neurons is relevant for their morphology where it acts as a negative regulator of axonal growth and branching.

Efa6 helps maintain axonal MT bundle integrity in cultured neurons

In our analyses we observed a further phenotype consisting in the regional loss of proper axonal MT bundle organisation due to MTs becoming non-coalescent and curled, particularly in mature neurons at 5 DIV (curved arrow in Fig. 2F).

Detailed analyses of the various Efa6-depleted conditions at 6 HIV indicated that the percentage of neurons showing any obvious patches of MT disorganisation was increased to 150-250% when normalised to wild-type controls (Fig. S2). Although many neurons showed some degree of visible MT disorganisation already at early stages, the extent of MT disorganisation in individual neurons tended to be fairly mild. To quantify the strength of this phenotype we used a more refined readout by measuring the area of MT disorganisation per axon area (referred to as 'MT disorganisation index', MDI) (Qu et al., 2017). MDI measurements revealed mild phenotypes in young neurons which gradually worsened thereafter: when normalised to wild-type, *Efa6*$^{GX6w-}$ and *Efa6*$^{KO\#1}$ mutant neurons showed an increase in MDI to only 151% ± 14SEM and 129% ± 26SEM at 6 HIV, a more pronounced rise to 164% ± 26SEM and 231% ± 43SEM at 5 DIV, and dramatic values of 288% ± 34SEM and 405% ± 55SEM at 10 DIV (Fig.4A-F,I; all normalised to controls). In contrast, over-expression of Efa6-FL::GFP in wild-type neurons caused a reduction of the MDI to 67% ± 8SEM at 6HIV and to 79% ± 4SEM at 5 DIV (Fig.4I), i.e. below baseline levels in control cells. Taken together, there was a higher likelihood for an early onset of MT disorganisation upon functional loss of Efa6, but cells displayed a modest degree of disorganisation at first which then gradually increased to pronounced phenotypes during the following days.

This gradual MDI increase might reflect maternal rescue, i.e. masking of the mutant phenotype caused by deposition of normal gene product from the healthy gene copy of the heterozygous mothers in the oocyte (Prokop, 2013b). To test this possibility, we used pre-culture strategies (Prokop et al., 2012; Sánchez-Soriano et al., 2010b) where cells were kept for 5 days in a tube before they were plated on a coverslip. However, we found that even upon such removal of Efa6 from earliest stages of axon growth, the MDI of *Efa6*$^{GX6w-}$ was low in young neurons but gradually increased to severe phenotypes over the following days (157% ± 18SEM at 6HIV; 297% ± 60SEM at 5 DIV; 577% ± 134SEM at 10DIV; normalised to wild-type controls; Fig.4J).

This finding argues for a continued role of Efa6 in preventing MT disorganisation during development as well as in mature neurons. To test continued requirement of Efa6 experimentally, we induced *Efa6* knock-down at a late stage around 3 DIV, when neurons have long undergone synaptic differentiation (Küppers-Munther et al., 2004; Prokop et al., 2012). For this, we used the temperature-controlled Gal80^{ts} system (see Materials and Methods) where the *Efa6-RNAi* knock-down construct is expressed only at elevated temperatures (27°C), but becomes repressed at lower temperatures (19°C). When *Efa6-RNAi* expression was blocked at 19°C for 3 days, the MDI of neurons was comparable to control neurons (Fig. 4K). When Efa6 was knocked-down thereafter for another 4 days (by shifting cells to 27°C for this period), the MDI of the experimental neurons was increased to 645% ±

94SEM, whereas the controls only showed a mild increase to ~277% (Fig. 4K). These data clearly indicate that MT disorganisation upon Efa6 deficiency occurs even in fully differentiated neurons and is not restricted to developmental stages.

<u>*Efa6* helps maintain axonal MT bundle integrity *in vivo*</u>

We then assessed whether a role of Efa6 in MT bundle maintenance is relevant *in vivo*. For this, we used the *GMR31F10-Gal4* driver line specific for a subset of lamina neurons in the adult optic lobe. These lamina neurons send axons into the medulla where they organise into highly stereotypic and clearly separable columns of axons (Prokop and Meinertzhagen, 2006) (Fig.5A). To label MTs in these lamina neurons, we used *GMR31F10-Gal4* in combination with *UAS-α-tubulin84B-GFP* either alone (*GMR-tub* controls) or together with *Efa6^{RNAi}* (*GMR-tub-Efa6^{IR}*) to knock down *Efa6* specifically in these neurons. When flies carrying these transgene combinations eclosed from their pupal cases, they were left to age for 26-27 days (about half their life expectancy) and then their brains were dissected out and analysed.

We found that Efa6 knock-down caused a doubling in the occurrence of axonal swellings containing disorganised axonal MTs: the average of total swellings per column section was increased from 0.3 in controls to 0.65 swellings upon Efa6 knock-down, and about a third of these contained disorganised MTs (*GMR-tub-Efa6^{IR}*: 0.23 per column section; *GMR-tub*: 0.13; Fig.5). These data suggested that our findings in cultured neurons are relevant *in vivo*.

Taken together, we identified three different morphological features that are regulated by Efa6: axon growth, axon branching and axonal bundle organisation. We therefore decided to study the underlying molecular mechanisms and performed subcellular analyses.

<u>Efa6 eliminates MTs in growth cones</u>

Based on the literature, Efa6 may cause these morphological effects through changes in the actin cytoskeleton, either as a potential activator of small Arf GTPases via its central Sec7 domain (D'Souza-Schorey and Chavrier, 2006; Huang et al., 2009), or through its other C-terminal domains (see below) (Derrien et al., 2002; Franco et al., 1999; Macia et al., 2008). Alternatively, it could act directly on MTs, as was suggested by studies of *Ce*Efa6 in oocytes where it acts as a membrane-associated MT elimination factor (also called cortical collapse factor) (O'Rourke et al., 2010). We first focussed on the latter possibility and studied potential effects of Efa6 on MT behaviours.

For this, we distinguished between different subcellular compartments of neurons, known to display very different behaviours: in the dynamically shaped, amoeboid growth cones (GCs) at the tips of growing axons, MTs splay out towards the membrane in the GC periphery (Prokop et al., 2013). In contrast, in the cable-like axon shafts, most MTs extend within bundles and are kept away from the membrane (Prokop, 2013a). If Efa6 acts as a cortical collapse factor, manipulations of its functions should therefore affect MTs in GCs and axon shafts differently. Consequently, we refined our approach by analysing these two sub-neuronal compartments separately, starting with GCs.

In GCs of *Efa6* mutant neurons at 6 HIV, the total number of Eb1 comets was increased when normalised to wild-type controls (fixed: 125% ± 7SEM; life: 135% ± 11SEM; Fig. 6I). Eb1::GFP comet velocity was unaffected (wildtype: 0.27µm/s ± 0.2SEM; *Efa6*: 0.30µm/s ± 0.2SEM), but their lifetime was ~1.4 times longer in mutant GCs (Fig. 6M). Compared to control neurons,

Eb1::GFP comets in *Efa6* mutant neurons appeared to vanish less often when reaching the GC periphery, where they could occasionally be observed to undergo persistent curved extensions along the periphery (Suppl. Movies not provided in this version).

We reasoned that, if there are more MTs in GCs of Efa6-depleted neurons, this should increase their chances of entering into filopodia. In agreement with this prediction, the percentage of tubulin-stained neurons displaying at least one MT in GC filopodia, was much higher upon loss of Efa6 (wild-type: 82%; *Efa6*: 97-98%; Fig.6L). Also the percentage of filopodia per neuron that contained Eb1 comets or tubulin-stained MTs, was considerably higher in GCs of *Efa6* mutant neurons as compared to controls (live Eb1::GFP: 151±4%; fixed Eb1: 123±6%; fixed tubulin ~150%; Fig.6J, K). In addition, the lifetime of Eb1 comets persisting at the tip of filopodia was increased from ~2 s in wildtype to ~6 s in *Efa6* mutant neurons (Fig. 6M). We even observed highly unusual cases where comets at the tip of filopodia moved backwards, seemingly pushed back by the retracting filopodial tip (Suppl. Movies not provided in this version).

Since the number of filopodia per GC was not obviously changed in the *Efa6* mutant neurons (~11 per neuron in wild-type and ~10 in *Efa6*), our data indicate that Efa6 negatively regulates the entry of MTs into GC filopodia, likely by eliminating their overall number and reducing their dwell time in filopodia. This interpretation was corroborated by experiments using *sca-Gal4* driven pan-neuronal expression of Efa6-FL::GFP. Like the endogenous protein, Efa6-FL::GFP localised to cell bodies, axons and growth cones (Figs.1B,C). But its increased levels upon over-expression caused phenotypes opposite to loss of Efa6 function (green bars in Fig.6): the amount of GC filopodia containing MTs was reduced to 49.7% ± 7SEM and the EB1 comet number in GCs and GC filopodia was reduced to 64% ± 4SEM and 57% ± 7SEM, respectively.

Overall, our data are in agreement with a role of Efa6 in eliminating growing MTs in the periphery of GCs. As is detailed in the discussion, the extension of MTs into filopodia matches the observed morphological phenotypes: filopodial entry of MTs is considered an important prerequisite for axon growth and can explain the observed changes in axon length (Prokop et al., 2013); it could also contribute to changes in branch numbers by promoting GC splitting events (Acebes and Ferrus, 2000).

<u>Efa6 eliminates MTs in axonal shaft filopodia</u>

When applying the same subcellular readouts to axon shafts, we found that loss or gain of Efa6 did not cause the strong effects on comet numbers and lifetimes that were observed in GCs of the same neurons. Instead these parameters were unaltered or only moderately changed relative to axon shafts of control neurons (numbers: 101% in *Efa6* fixed, 108% in *Efa6* live; 89% in Efa6-FL::GFP fixed; average lifetime: 102%, all data normalised to wild-type controls; Fig. 7A,B). Along these lines, also the percentages of comets moving antero- *versus* retrogradely, was unchanged (~75% *versus* ~25%; Fig. 7D).

Other values were comparable to GCs. Firstly, like GCs, also axon shafts displayed no obvious changes in comet velocities (Fig.7C; average velocity: 107%; normalised to controls). Secondly, like in GCs, there was a strong increase in MTs entering filopodia along axon shafts. When assessing the percentage of neurons displaying at least one Eb1 comet or tubulin-stained MT extending into shaft protrusions, the numbers were doubled in Efa6-deficient neurons and drastically reduced when expressing Efa6-FL::GFP (Eb1 / tubulin for wt: ~17% / ~33%; for *efa6*: ~42% / ~61%; for Efa6-FL::GFP: ~8% / ~15%; Fig.7E,F). Also the

percentage of filopodia per neuron that contained Eb1 comets or tubulin-stained MTs (6% in wild-type) was increased ~15-fold in *Efa6* mutant neurons (even when normalised to axon length; 0.05 MTs/µm of axon length in wild-type), whereas Efa6-FL::GFP caused a strong reduction relative to control neurons (details in Fig. 7G,H).

Taken together, also our findings in axon shafts are consistent with a model in which Efa6 eliminates MTs at the cortex. However, Efa6 seems not to influence MTs which are kept in axonal bundles (likely through independent mechanisms involving MT-MT cross-linkage or Shot-mediated guidance; see Introduction). In this scenario, Efa6 would provide a quality control mechanism eliminating only MTs that escaped axonal bundles - which would also be consistent with the slow onset and gradual increase of MT disorganisation we observed (Fig.4I,J). Increases in off-track MTs are also considered a prerequisite for interstitial branch formation (Kalil and Dent, 2014; Lewis et al., 2013) and could therefore contribute to the branching phenotypes observed (Figs.2 and 3).

The N-terminus of Efa6 can eliminate whole axons in neurons

We next established which region of the Efa6 protein carries MT eliminating capabilities. For this, we first analysed Efa6 proteins from 30 species using Bayesian inference of phylogenetic relationships (via MrBayes) (Ronquist et al., 2012). These analyses revealed that all chordate proteins are rather distant from invertebrates, where arthropods form a clear subgroup within (Fig. S3A). When aligning the Efa6 proteins, the C-terminal halves appear relatively consistent, in most species containing a putative pleckstrin homology (PH; potential membrane association) (Macia et al., 2008), Sec7 (potential activation of ARF GTPases) and coiled-coil (CC) domain (Franco et al., 1999) (Fig.8A, S4). In contrast, the N-terminus is mainly unstructured and reveals enormous length differences among species; notably, phylogenetic relationship analyses with the N-terminus alone reveal a very similar tree as the full length comparison (Fig. S3A,B). We therefore generated two complementary constructs which reflect these two very different parts of Efa6: *Efa6-ΔCterm-GFP* encoding the entire N-terminal half upstream of the Sec7 domain, and *Efa6-ΔNterm-GFP* encoding the rest of the protein.

To functionally assess these Efa6 variants, we developed a transfection method for *Drosophila* primary neurons (see Methods) and validated it by transfecting *Efa6-FL-GFP*. When analysing these transfected primary neurons, we found that they had the same sub-cellular localisation and reduced axon length phenotypes as observed in neurons expressing Efa6-FL::GFP from transgenic constructs (Figs.1C, S5B, 2C,D).

Having established this technique, we transfected *Efa6-ΔCterm::GFP* or *Efa6-ΔNterm::GFP*. Both variants localised throughout neurons (Fig.S5C,H), but only the N-terminus induced obvious phenotypes. Notably, the phenotypes induced by Efa6-ΔNterm::GFP were considerably stronger than observed with Efa6-FL::GFP, in that axons were severely reduced or frequently even absent. To quantify potential axon loss, we labelled neurons with the pan-neuronal marker Elav (Robinow and White, 1991) and found that only ~36% had an axon when expressing Efa6-ΔCterm::GFP, as compared to ~57% with Efa6-FL::GFP, ~74% with GFP and 74% with Efa6-ΔNterm::GFP (Fig.8B).

These results clearly indicate that MT-eliminating functions reside in the N-terminus whereas C-terminal domains appear dispensable to this end. Of these, the Sec7 domain is expected to activate Arf6 (Huang et al., 2009), but also removal of Arf6 function from primary neurons

(*Arf51F*$^{GX16[w-]}$ null mutant allele) had no obvious effects on axon morphology (data not shown).

Membrane association of the C-terminus restricts MT elimination to the membrane cortex

As described above, the power of Efa6-ΔCterm::GFP in eliminating axons is considerably greater than observed with EFA6-FL::GFP. This is likely due to the fact that Efa6-ΔCterm::GFP lacks the membrane-associating PH domain, so that it can diffuse into the core area of axons and eliminate MTs that are usually out of reach for the full length Efa6 protein.

To test this possibility, we generated two constructs: one encoding a shorter N-terminal variant of Efa6 (*Efa6-Nterm-GFP*; Fig.8B) and another where this variant was fused to a membrane-associating CAAX domain (Hancock et al., 1991) (*Efa6-Nterm-GFP-CAAX*; Fig.8B). Both variants localised throughout neurons (Fig.S5D,I). However, Efa6-Nterm::GFP showed the same strong axon-abolishing effects as observed with Efa6-ΔCterm::GFP, whereas the phenotypes induced by the Efa6-Nterm::GFP::CAAX variant were much weaker (Fig.8B). These findings suggest that membrane tethering of the Efa6 N-terminus lowers the harmful effects it has in axons. This said, axon-abolishing effects of the CAAX construct were slightly higher than with Efa6-FL::GFP, but this might be due to the fact that membrane association properties of CAAX differ from the PH domain of Efa6 (Fig.8B). Correlating with this notion, we found that transgenically expressed Efa6-Nterm::GFP::CAAX also caused a slightly stronger reduction in axonal side branches at 5DIV than observed with the Efa6 full length variant (Efa6-FL: 79%; Efa6-Nterm-CAAX: 79±4%; Fig. 2H,I).

To complement these studies and achieve a higher subcellular resolution, we used NIH3T3 mouse fibroblasts as suitable heterologous cellular models for the study of *Drosophila* proteins (Alves-Silva et al., 2012). 24 hrs after transfection, fibroblasts with moderate Efa6-FL::GFP expression showed strong GFP staining along the circumference and in areas of membrane folds, indicative of membrane association (open arrow heads and curved arrow in Figs.S6B and S7B). Membrane association was further suggested by a strong membrane ruffle phenotype (curved arrows in Figs.S8B), which was similarly observed when expressing human Efa6 homologues (Fig.S8E) (Derrien et al., 2002; Franco et al., 1999; Macia et al., 2008). With increasing expression levels, Efa6-FL::GFP was also found in the cytoplasm, suggesting that membrane-association might become saturated (Fig.S7C). Consistent with these observations, we found a concentration-dependent MT depletion effect, with higher Efa6-FL expression levels leading to more severe MT loss (Fig. S7D). Notably, MTs have a strong tendency to vanish along the cell fringes, further suggestive of predominantly membrane-based MT elimination. In total, 25% of transfected cells were normal, 59% displayed depletion of MTs from the fringes, and a small fraction of 16% had an almost complete loss of MTs (Figs.8B, S9B).

When transfecting *Efa6-ΔCterm-GFP* or *Efa6-Nterm-GFP* expression constructs, MT depletion was more than doubled (Fig. 8B). As expected, the expressed proteins failed to localise to membranes; even at low expression levels, they were found exclusively in the cytoplasm and the nucleus (double chevrons in Fig.S6C,D) - of which the nuclear localisation is a known phenomenon for GFP-tagged proteins (Alves-Silva et al., 2012; Seibel et al., 2007) and not necessarily caused by the N-terminal sequence. When using the N-terminal construct fused to CAAX, the construct re-associated to membranes: Efa6-Nterm::GFP::CAAX revealed a similar localisation at cell edges and absence from the nucleus as observed with Efa6-FL::GFP (Figs. S6B,I). Also the MT depletion phenotype was far milder with the CAAX variant

(Fig. 8B), thus corroborating our findings in neurons.

Finally, the Efa6-ΔNterm::GFP variant localised to the plasma membrane in fibroblasts and was found in the cytoplasm only upon increased expression levels (Fig.S6H). But even at high levels, it had no obvious effects on MT networks, and cells were indistinguishable from GFP-transfected controls (Fig.8B). Notably, we observed that Efa6-ΔNterm::GFP induced strong membrane ruffling, as we had similarly observed with the full length construct of Efa6 and human PSD(1) (Fig. S8B,D,E). This suggests conserved roles of the C-terminus in cortical actin regulation, because also the human Efa6 homologues PSD(1) and PSD4 use their C-terminal PH and CC domains to induce actin cytoskeletal re-organisation and membrane ruffle formation in TRVb-1 and baby hamster kidney cells (Derrien et al., 2002; Franco et al., 1999; Macia et al., 2008).

Taken together, various findings are in agreement with a model where endogenous Efa6 displays MT eliminating functionality in its N-terminus which is restricted to the cortex via its C-terminus. These findings include (1) the milder MT phenotypes of CAAX and FL variants *versus* the ΔCterm or Nterm variant, (2) the membrane association in fibroblasts, and (3) the type of morphological and MT phenotypes we observed.

<u>The putative PDZ domain and functional SxIP motifs are not required for MT elimination</u>

We next aimed to identify the motifs in the N-terminus required for MT elimination. The N-terminal half of the *Drosophila* Efa6 protein is mostly unstructured and comprises almost 900 amino acids (aa), which is unusually long compared to most other species (Figs. 8A,C and S4A). Our CAAX-related experiments with the 410 aa long Efa6-Nterm::GFP variant had already shown that most if not all MT-eliminating function localises to this stretch of the protein which contains three different domains/motifs (Fig.8A,B): a putative PDZ domain (aa16-88), two SxIP motifs surrounded by positive charges (aa 233-6 and 262-5), and a motif of 18aa displaying 89% similarity with a motif in the N-terminus of *Ce*Efa6 (O'Rourke et al., 2010).

Of these, PDZ domains usually provide anchorage to transmembrane proteins (Ponting et al., 1997), but might not do so in Efa6 because the N-terminus seems to fail to attach to membranes in neurons and fibroblasts (Fig.S6C,D). Furthermore, detailed phylogenetic analyses of the N-terminus using the EMBL SMART prediction service (Letunic and Bork, 2018), revealed that the PDZ domain seems to be a feature mainly of insect versions of Efa6 (Fig.S4A). We therefore did not analyse it further.

SxIP motifs tend to mediate binding to Eb1 if surrounded by positive charges (Honnappa et al., 2009), and such a function could potentially aid in capturing MTs for elimination. The SxIP sites of Efa6 seem indeed to be functional, since we found that fibroblasts expressing Efa6-Nterm::GFP displayed clear cases of MT tip tracking behaviour, but only in some very rare cases where MTs had not yet been abolished by the construct (Suppl. Movie S7). To test whether these SxIP motifs are relevant for MT-eliminating functions of Efa6, we generated an *Efa6-Nterm$^{\Delta SxIP}$::GFP* variant in which those motifs were mutated to four alanins. Live imaging of fibroblasts transfected with this construct never revealed any comet formation, but anti-GFP and -tubulin staining of fibroblasts or primary *Drosophila* neurons revealed the same general localisation as well as axon or MT defects as observed with Efa6-Nterm::GFP (Figs.8B, S5E, S6E). Therefore, Eb1 interaction does not appear a major requirement for Efa6-mediated MT elimination. In agreement with this finding, SxIP motifs are also not widely conserved in other species, and we could only identify them in a subset of insects (primarily flies) and molluscs, and a derived SxLP motif in a number of

vertebrate/mammalian species (Fig. S4A).

A conserved MT binding domain is crucial for MT-elimination

We next analysed the conserved 18aa motif (T10), because its worm homologue is known to display MT-eliminating properties (O'Rourke et al., 2010). To assess potential roles of this putative MT-eliminating domain (MTED) in the *Drosophila* Efa6 N-terminus, we generated two more expression constructs (Fig. 8B): Efa6-Nterm$^{\Delta MTED}$-GFP (truncated immediately before the MTED) and Efa6-MTED-GFP (consisting of only the MTED).

When transfected into neurons, both constructs were expressed in cell bodies and throughout axons, as had been similarly observed for Efa6-Nterm::GFP (Fig.S5D,F,G). Also in fibroblasts, they all showed a comparable localisation diffusely in the cytoplasm and strongly in the nucleus (Fig.S6D,F,G). However, the phenotypes they induced were very different from each other, but consistent between neurons and fibroblasts (Fig.8B): in contrast to the strong elimination of neuronal axons and fibroblast MT networks we had observed with Efa6-Nterm::GFP (Figs.S5D and S9D), Efa6-Nterm$^{\Delta MTED}$::GFP caused no obvious phenotypes (Figs.S5F, S9G). In contrast, MTED::GFP alone was sufficient to cause severe loss of axons and fibroblast MTs, although these effects were milder than with Efa6-Nterm::GFP (Fig.8B). Notably, transfection rates with *Efa6-MTED-GFP* in fibroblasts were consistently very low and cell densities were reduced compared to controls, suggesting that MTED induces cell lethality through an unknown mechanism. These data clearly indicated the MTED as a key domain required for Efa6-induced MT elimination.

Surprisingly, our phylogenetic analyses revealed that also the MTED domain was not well conserved across the animal kingdom; it was predicted primarily for nematodes, arthropods and molluscs (Fig. S4A). To further complement this finding, we deduced a MTED consensus sequence from 39 *Efa6* genes (details in Fig.S4B, T10), identified the most likely human MTED-like sequence [position 31-49aa of PSD(1); Fig. 8A] and synthetically generated GFP-tagged constructs codon-optimised for expression in mammalian cells; as positive controls we generated codon-optimised constructs encoding MTEDs of fly and *C. elegans* (Fig. 8E). In addition, we generated expression constructs containing human *PSD(1)-Nterm-GFP*, *CeEfa6-Nterm-GFP* (Fig. 8D), as well as the full length sequences of *CeEfa6* or the four human *PSD* genes (Fig. 8C) - all to be used alongside their fly counterparts. When transfected into fibroblasts all three fly and all three worm constructs had strong MT eliminating properties, whereas none of the 6 human constructs showed any such effect (Fig.8C-E). These data suggest that the presence of a well conserved canonical MTED seems to be a good predictor for MT eliminating capabilities of Efa6 proteins.

We therefore carried out a series of experiments to unravel the mechanism through which MTEDs act. However, experiments with purified Efa6-Nterm::GFP as well as synthetically generated MTED were not able to reproduce MT-destabilising functions in *in vitro* assays: neither with GMPCPP-stabilised MTs (although binding of Efa6-ΔCterm::GFP to MTs was observed; Fig.S10A,B), nor with MTs in *Xenopus* oocyte extracts (Fig.S10C,D). The latter was especially surprising because mRNA injections of *Efa6-Nterm-GFP* mRNA into *Xenopus* eggs generated cell division defects expected of a MT destabiliser (Fig.S1F).

Taken together, Efa6-mediated MT elimination is driven solely or primarily by the MTED motif, through a mechanism that remains elusive at present. Although this motif and its functions are restricted to invertebrates, the phenotypes associated with Efa6-mediated MT elimination in *Drosophila* neurons offer unique opportunities to develop a conceptual model for how known

neuronal cortical collapse factors, such as mammalian Kif21A (van der Vaart et al., 2013), may contribute to disease-relevant aspects of axon morphology and maintenance.

Efa6 and Shot cooperate in MT bundle formation and maintenance

As a fundamental conceptual model for axonal MTs, we recently proposed the hypothesis of "local axon homeostasis". It proposes that the high-force environment inside axons causes MTs to become disorganised by default, and that MT regulators are required to 'tame' them into bundles (Prokop, 2016; Voelzmann et al., 2016a). In this model, the cortical MT-elimination function of Efa6 could serve as a quality control mechanism, eliminating off-track MTs that have accidentally left the bundle.

To test this possibility, we made use of spectraplakins, which are the most prominent neuronal factors required for the bundled organisation of axonal MTs (Voelzmann et al., 2017). In *Drosophila*, spectraplakins are represented by the single *short stop* (*shot*) gene, and its functional loss in *Drosophila* primary neurons causes a severe increase in axonal off-track MTs (Alves-Silva et al., 2012). Accordingly, the MDI value of $shot^{3}$ mutant neurons was rather high (239% ± 14SEM normalised to wild-type controls) if compared to the $Efa6^{GX6[w-]}$ mutant phenotype at that same stage (155% ± 14SEM ; Fig. 4M). It was even further increased in $shot^{3}$ $Efa6^{GX6[w-]}$ double mutant neurons (416% ± 24SEM), with an increment a third higher than the added increment of the single mutant conditions. The increase of MT disorganisation in the double-mutant over the single mutant condition is consistent with a scenario in which Efa6 eliminates a substantial fraction of the aberrant off-track MTs caused by loss of Shot; the fact that Shot deficiency alone shows MT disorganisation might indicate that this function of Efa6 becomes saturated by the sheer amount of off-track MTs generated under this condition (Fig. 9).

In a complementary strategy, we expressed *Efa6-RNAi* in a $shot^{3/+}$ heterozygous mutant background, and found that the MDI was clearly enhanced both at 6HIV and 5 DIV ($shot^{3/+}$: 126% ± 12SEM; *Efa6-RNAi*: 130% ± 13SEM; $shot^{3/+}$ *Efa6-RNAi*: 173% ± 13SEM; Fig. 4L). This enhancement was also observed *in vivo* (Fig.4L). For this, we capitalised on the optic lobe model using *GMR31F10-Gal4* together with *UAS-α-tubulin84B-GFP* to label MTs in a subset of lamina neurons (*GMR-tub*). In our original experiment, *GMR-tub* had been combined with $UAS\text{-}Efa6^{RNAi}$ to knock down *Efa6* specifically in these neurons ($GMR\text{-}tub\text{-}Efa6^{IR}$). Here we combined *GMR-tub* with $shot^{3/+}$ mutant background to assess the baseline phenotype of the *shot* heterozygous mutant condition (*GMR-tub* $shot^{3/+}$) and, in parallel, with $UAS\text{-}Efa6^{RNAi}$ plus *shot* heterozygous mutant background to assess potential enhancement of mutant phenotypes if both conditions are combined ($GMR\text{-}tub\text{-}Efa6^{IR}$ $shot^{3/+}$). We observed 0.30 / 0.13 swellings per column section (total / with MT disorganisation) in *GMR-tub* control flies, 0.67 / 0.19 swellings in *GMR-tub* $shot^{3/+}$ flies, 0.65 / 0.23 swellings in $GMR\text{-}tub\text{-}Efa6^{IR}$ flies and 0.97 / 0.49 swellings in $GMR\text{-}tub\text{-}Efa6^{IR}$ $shot^{3/+}$ flies where both conditions are combined (Fig.5). These data show a strong enhancement of the MT disorganisation phenotype, suggesting that Efa6 and Shot perform complementary functions that contribute to axonal MT bundle maintenance also *in vivo*.

Discussion

Efa6 is an essential component of the machinery that regulates MT behaviours underpinning

axon morphology

Axons are the structures that wire the brain, fundamental to nervous system function. To understand how axons are formed during development, maintained in a plastic state thereafter but also pushed into degeneration by pathological conditions, we need more profound knowledge of the axonal MT bundles at their core, and how they are regulated by MT-binding proteins (Voelzmann et al., 2016a). Here we show that the cortical collapse factor Efa6 is required for these bundled MT arrangements. We propose that Efa6 acts as a quality control factor which eliminates accidental off-track MTs that extend away from the MT bundle towards the axonal plasma membrane.

This function of Efa6 can be inferred from integrating various complementary observations: (1) Efa6 loss induces phenotypes in neurons that comprise an increase in Eb1 comet numbers specifically in GCs, and a rise in MTs entering filopodia throughout axons. (2) Upon loss of Efa6, MTs have longer half-lives and gradually arrange into winding trajectories instead of parallel ones. (3) Over-expression of Efa6-FL::GFP fundamentally inverts the above phenotypes. (4) Speed and antero- *versus* retrograde directionality of MT polymerisation events are unaffected in Efa6-deficient neurons, indicating that Efa6 is not an instructive regulator of these events. (5) Structure-function analyses of Efa6 in neurons and fibroblasts demonstrate its compartmentalised ability to eliminate MTs at the membrane.

Figure 10 demonstrates how all these findings can be integrated into a consistent model, based on our current knowledge of MT behaviours in GCs (Dent and Gertler, 2003; Prokop et al., 2013), and on our own hypothesis of 'local axon homeostasis' describing MTs in axon shafts (Fig.9A) (Prokop, 2016; Voelzmann et al., 2016a). We propose that Efa6-mediated cortical MT elimination exists in a well-balanced equilibrium, sufficient to eliminate occasional off-track MTs (thus preventing MT disorganisation), but still permitting intended morphogenetic changes, such as axon growth or branching. Both these morphogenetic events are enhanced upon loss of Efa6 and reduced upon Efa6 over-expression, further illustrating the balanced nature of the system. Such a model where active mechanisms maintaining MTs in bundles protect them against cortical collapse would also solve the long known conundrum of how axonal MTs extend hundreds of micrometres in the immediate vicinity of the cell cortex in axons, whereas they tend to interact with the cortex in non-neuronal cells by being either eliminated or captured (Fukata et al., 2002; Kaverina et al., 1998).

Roles of Efa6 during axonal growth, branching and MT bundle maintenance

In the case of axon growth, MTs constantly polymerise towards the periphery of GCs and a fraction of them overcomes elimination and enters filopodia; such events may also be actively regulated by guidance mechanisms, such as drebrin-Eb3 cross-linkage (Geraldo et al., 2008). MTs entering filopodia have the chance of actively contributing to axon extension; this is consistent with the widely accepted protrusion-engorgement-consolidation model of axon growth which proposes that stabilised MTs in filopodia can seed axon elongation events (Aletta and Greene, 1988; Goldberg and Burmeister, 1986; Prokop et al., 2013). Loss of Efa6 would favour this mode of growth (and thus explain increased axon length observed in these neurons) in two ways: through allowing more MTs to enter filopodia, and through allowing them to dwell in filopodia for longer thus enhancing the likelihood of their stabilisation (yellow arrows in Fig.9C). Furthermore, this scenario would explain why loss of *Efa6* in *C. elegans* improves axon re-growth after injury and growth overshoot during development (Chen et al., 2015; Chen et al., 2011). It would also provide a mechanism that can explain enhanced branching of Efa6-deficient neurons, since entry of multiple MTs in filopodia may cause simultaneous growth events in the same GC, thus leading to GC splitting as one mode of

branch formation (yellow arrows on the right in Fig.9C) (Acebes and Ferrus, 2000).

Axon branching can also occur along axon shafts, although a number of mechanisms (including Efa6) prevents this through keeping MTs in bundled conformation (Fig.9A). This is consistent with current models proposing that collateral branching requires the active generation (e.g. through MT severing) and stabilisation of off-track MTs that can enter shaft filopodia (Kalil and Dent, 2014; Lewis et al., 2013; Yu et al., 2008). This scenario bears reminiscence with greater numbers of MTs in shaft filopodia observed in *Efa6* mutant neurons at 6 HIV, which then correlate with enhanced axonal branch numbers in mature neurons, in culture and in the brain *in vivo* (red arrow in Fig.9C); this effect was inverted upon Efa6 over-expression. It seems therefore that also interstitial branch formation may contribute to the observed phenotypes. It remains to be seen whether branching events require active regulation of Efa6, for example through signalling events triggering sub-cellular re-localisation of Efa6 away from this site (Chen et al., 2015) or the functional inactivation of Efa6. But the simplest mode would be that Efa6 is homogeneously distributed at well-balanced concentrations, so that the sheer increase in off-track MTs can outnumber Efa6-mediated elimination (Fig.9D).

This latter observation is supported by increased off-track MTs in *shot* mutant neurons: Efa6 can eliminate many of these, as is indicated by enhanced phenotypes in *shot Efa6* double-mutant neurons as compared to neurons lacking only Shot; it is also indicated by the shortened lifetime of MT comets observed in *shot* mutant neurons (Alves-Silva et al., 2012). However, Efa6 is not sufficient to eliminate all off-track MTs in *shot* mutant neurons, thus explaining their severe MT disorganisation. In neurons lacking only Efa6, MT disorganisation is initially modest, likely due to the fact that off-track MTs are rare events, but they appear to accumulate over time, thus explaining the gradual increase in MT disorganisation we observed (Fig.4I,J). The late onset upon conditional knock-down we observed, makes sense if considering that MT polymerisation continues in mature neurons as a mechanism to prevent senescence of axonal MT bundles (Qu et al., 2017; Voelzmann et al., 2016a).

Clearly, the MT disorganisation phenotypes are far less pronounced *in vivo* than in culture, but this is expected when considering that axons *in vivo* tend to be arranged into closely adhered nerve tracts and surrounded by glial cells, i.e. have a much more rigid plasma membrane and cortex, able to resist MTs pushing out to form swellings and areas of disorganisation.

Evolutionary and mechanistic considerations of Efa6 function

We found that the mammalian Efa6 proteins encoded by four *PSD* genes, do not contain a canonical MTED and lack any MT collapse function. However, we propose that comparable functional contributions are taken over by different types of cortical MT collapse factors. For example, the kinesin-4 family member Kif21A was shown to act as a cortical collapse factor and is expressed throughout neurons in mammals (van der Vaart et al., 2013). The R954W mutation of Kif21A links to the eye movement disorder 'congenital fibrosis of extraocular muscles' (OMIM reference #135700) (Tiab et al., 2004) and was shown to cause a shift of the proteins localisation in cultured hippocampal neurons from axons towards GCs, expected to cause a loss-of-function in the axon and gain-of-function in GCs (van der Vaart et al., 2013). Increased protein levels in GCs correlate with reduced axon growth (as similarly observed with Efa6 over-expression); decreased levels in proximal axons correlate with a local increase in side branches (as similarly observed upon Efa6 loss-of-function). Therefore, our findings with Efa6 can serve as a paradigm to guide research into the disease-relevant roles of cortical

collapse factors in higher organisms.

Our studies together with previous work on *Ce*Efa6 (O'Rourke et al., 2010) clearly indicate a central role for the MTED in MT elimination, but the molecular mechanisms through which they perform this function remain unfortunately elusive for now. In principle, MT elimination can occur from their ends (like kinesin-8 or the kinesin-13 Kif2/MCAK) (Brouhard and Rice, 2014) or by destroying MTs along their shafts (like katanin or spastin) (Sharp and Ross, 2012). It can be achieved by depolymerisation, severing, buckling and breaking, or extrusion of tubulins along their shafts. Since the MTED is only a very short peptide, it would not be surprising if it acted indirectly through other MT regulators, which is why in addition to our studies *in vitro* we carried out analyses in *Xenopus* oocyte extracts (Fig. S10C); for example, it could activate MT destabilisers or block polymerisation processes. In any case, the small size of MTEDs might come in handy as experimental tools to eliminate MTs, with potentially complementary properties to existing factors such as kinesin-13s (Moore et al., 2005; Schimizzi et al., 2010), Stathmin (Marklund et al., 1996), Spastin or Katanin (Eckert et al., 2012; Trotta et al., 2004).

In contrast, other regions of the Efa6 N-terminus are poorly conserved even among invertebrates and seem not to contribute to MT elimination in prominent ways. For example, SxIP sites of Efa6 mediate plus end tracking (Suppl. Movies not provided in this version), and MT plus end capture seemed an attractive candidate mechanism to facilitate cortical MT collapse. However, we found the SxIP sites to be dispensable for MT elimination (Fig.8B), and our *in silico* analyses of Efa6 proteins failed to reveal any other Eb1-binding motifs, such as CAP-Gly or LxxPTPh sites (Akhmanova and Steinmetz, 2008; Kumar et al., 2017). The scenario for Efa6 appears therefore comparable to that of MCAK which is a prominent tip-tracker but does not require this property for its MT depolymerising activity (Moore et al., 2005).

In contrast to the N-terminus, the C-terminal domains of Efa6 seem to display some degree of functional conservation. So far, work on mammalian PSDs has revealed functions for C-terminal domains in regulating ARF6, ARF1 or ARL14 during actin cytoskeletal reorganisation, tumour formation and immune regulation (Derrien et al., 2002; Paul et al., 2011; Pils et al., 2005). Our finding that PSD(1) and C-terminal Efa6 constructs cause similar membrane ruffling phenotypes in fibroblasts (Figs.S6 and S8) suggests that some conserved functions reside in this region and might contribute, together with N-terminally mediated MT collapse, to the neuronal or non-neuronal defects that cause semi-lethality displayed by *Efa6* mutant flies (data not shown).

Main conclusions and future perspectives

We propose Efa6 to act as a cortical collapse factor which is important for the regulation of axonal MTs and, in turn, axon growth, maintenance and branching. Although this function is evolutionarily not widely conserved, our findings provide a helpful paradigm for studies on other classes of cortical collapse factors also in mammalian neurons. Further important research avenues will be to identify the mechanism of Efa6-mediated MT elimination, not only to better understand how it can be regulated in axons but also to explore potential roles for MTEDs as molecular tools in cell biological research.

Acknowledgements

This work was made possible through funding by the BBSRC (BB/I002448/1, BB/P020151/1, BB/L000717/1, BB/M007553/1) to A.P., by parents as well as the Faculty of Life Sciences to Y.Q., by the Leverhulme Trust to I.H. (ECF-2017-247), by the German Research Council (DFG) to A.V. (VO 2071/1-1), and by the BBSRC to N.S.S. (BB/M007456/1) and KD (BB/J005983/1). The Manchester Bioimaging Facility microscopes used in this study were purchased with grants from the BBSRC, The Wellcome Trust and The University of Manchester Strategic Fund. The Fly Facility has been supported by funds from The University of Manchester and the Wellcome Trust (087742/Z/08/Z). We thank Tom Millard for very helpful comments on the manuscript, Simon Lowell for advice on the phylogenetic analyses,Hiro Ohkura for kindly providing DmEb1 antibody and Andrew Chisholm for the C.elegans Efa6 and human PSD constructs. Stocks obtained from the Bloomington *Drosophila* Stock Center (NIH P40OD018537) were used in this study.

References

Abascal, F., Zardoya, R., and Posada, D. (2005). ProtTest: selection of best-fit models of protein evolution. Bioinformatics *21*, 2104-2105.

Acebes, A., and Ferrus, A. (2000). Cellular and molecular features of axon collaterals and dendrites. Trends Neurosci *23*, 557-565.

Adalbert, R., and Coleman, M.P. (2012). Axon pathology in age-related neurodegenerative disorders. Neuropathol Appl Neurobiol *39*, 90–108.

Akhmanova, A., and Steinmetz, M.O. (2008). Tracking the ends: a dynamic protein network controls the fate of microtubule tips. Nat Rev Mol Cell Biol *9*, 309-322.

Aletta, J.M., and Greene, L.A. (1988). Growth cone configuration and advance: a time-lapse study using video-enhanced differential interference contrast microscopy. J Neurosci *8*, 1425-1435.

Allan, V.J. (1993). Assay of membrane motility in interphase and metaphase Xenopus extracts. Methods Cell Biol *39*, 203-226.

Allan, V.J., and Vale, R.D. (1991). Cell cycle control of microtubule-based membrane transport and tubule formation in vitro. J Cell Biol *113*, 347-359.

Alves-Silva, J., Sánchez-Soriano, N., Beaven, R., Klein, M., Parkin, J., Millard, T., Bellen, H., Venken, K.J.T., Ballestrem, C., Kammerer, R.A.*, et al.* (2012). Spectraplakins promote microtubule-mediated axonal growth by functioning as structural microtubule-associated proteins and EB1-dependent +TIPs (Tip Interacting Proteins). J Neurosci *32*, 9143-9158.

Bernier, G., and Kothary, R. (1998). Prenatal onset of axonopathy in Dystonia musculorum mice. Dev Genet *22*, 160-168.

Bettencourt da Cruz, A., Schwarzel, M., Schulze, S., Niyyati, M., Heisenberg, M., and Kretzschmar, D. (2005). Disruption of the MAP1B-related protein FUTSCH leads to changes in the neuronal cytoskeleton, axonal transport defects, and progressive neurodegeneration in *Drosophila*. Mol Biol Cell *16*, 2433-2442.

Brouhard, G.J., and Rice, L.M. (2014). The contribution of aß-tubulin curvature to microtubule dynamics. J Cell Biol *207*, 323-334.

Chen, L., Chuang, M., Koorman, T., Boxem, M., Jin, Y., and Chisholm, A.D. (2015). Axon injury triggers EFA-6 mediated destabilization of axonal microtubules via TACC and doublecortin like kinase. eLife *4*, e08695.

Chen, L., Wang, Z., Ghosh-Roy, A., Hubert, T., Yan, D., O'Rourke, S., Bowerman, B., Wu, Z., Jin, Y., and Chisholm, A.D. (2011). Axon regeneration pathways identified by systematic genetic screening in *C. elegans*. Neuron *71*, 1043-1057.

Crooks, G.E., Hon, G., Chandonia, J.M., and Brenner, S.E. (2004). WebLogo: a sequence logo generator. Genome Res *14*, 1188-1190.

D'Souza-Schorey, C., and Chavrier, P. (2006). ARF proteins: roles in membrane traffic and beyond. Nature Rev Molec Cell Biol *7*, 347.

Dalpe, G., Leclerc, N., Vallee, A., Messer, A., Mathieu, M., De Repentigny, Y., and Kothary, R. (1998). Dystonin is essential for maintaining neuronal cytoskeleton organization. Mol Cell Neurosci *10*, 243-257.

Darriba, D., Taboada, G.L., Doallo, R., and Posada, D. (2011). ProtTest 3: fast selection of best-fit models of protein evolution. Bioinformatics *27*, 1164-1165.

Debanne, D., Campanac, E., Bialowas, A., Carlier, E., and Alcaraz, G. (2011). Axon physiology. Physiol Rev *91*, 555-602.

Dent, E.W., and Gertler, F.B. (2003). Cytoskeletal dynamics and transport in growth cone motility and axon guidance. Neuron *40*, 209-227.

Derrien, V., Couillault, C., Franco, M., Martineau, S., Montcourrier, P., Houlgatte, R., and Chavrier, P. (2002). A conserved C-terminal domain of EFA6-family ARF6-guanine nucleotide exchange factors induces lengthening of microvilli-like membrane protrusions. Journal of cell science *115*, 2867-2879.

Eckert, T., Le, D.T.-V., Link, S., Friedmann, L., and Woehlke, G. (2012). Spastin's microtubule-binding properties and comparison to katanin. PLoS One *7*, e50161.

Elliott, S.L., Cullen, C.F., Wrobel, N., Kernan, M.J., and Ohkura, H. (2005). EB1 is essential during *Drosophila* development and plays a crucial role in the integrity of chordotonal mechanosensory organs. Mol Biol Cell *16*, 891-901.

Eva, R., Koseki, H., Kanamarlapudi, V., and Fawcett, J.W. (2017). EFA6 regulates selective polarised transport and axon regeneration from the axon initial segment. Journal of cell science *130*, 3663-3675.

Fang, Y., and Bonini, N.M. (2012). Axon degeneration and regeneration: insights from *Drosophila* models of nerve injury. Annu Rev Cell Dev Biol *28*, 575-597.

Fassier, C., Tarrade, A., Peris, L., Courageot, S., Mailly, P., Dalard, C., Delga, S., Roblot, N., Lefevre, J., Job, D.*, et al.* (2013). Microtubule-targeting drugs rescue axonal swellings in cortical neurons from spastin knockout mice. Dis Model Mech *6*, 72-83.

Ferrier, A., Boyer, J.G., and Kothary, R. (2013). Cellular and molecular biology of neuronal Dystonin. Int Rev Cell Mol Biol *300*, 85-120.

Fiala, J.C., Feinberg, M., Peters, A., and Barbas, H. (2007). Mitochondrial degeneration in dystrophic neurites of senile plaques may lead to extracellular deposition of fine filaments. Brain Struct Funct *212*, 195-207.

Franco, M., Peters, P.J., Boretto, J., van Donselaar, E., Neri, A., D'Souza-Schorey, C., and Chavrier, P. (1999). EFA6, a sec7 domain-containing exchange factor for ARF6, coordinates membrane recycling and actin cytoskeleton organization. EMBO J *18*, 1480-1491.

Fukata, M., Watanabe, T., Noritake, J., Nakagawa, M., Yamaga, M., Kuroda, S., Matsuura, Y., Iwamatsu, A., Perez, F., and Kaibuchi, K. (2002). Rac1 and Cdc42 capture microtubules through IQGAP1 and CLIP-170. Cell *109*, 873–885.

Geraldo, S., Khanzada, U.K., Parsons, M., Chilton, J.K., and Gordon-Weeks, P.R. (2008). Targeting of the F-actin-binding protein drebrin by the microtubule plus-tip protein EB3 is required for neuritogenesis. Nat Cell Biol *10*, 1181-1189.

Goldberg, D.J., and Burmeister, D.W. (1986). Stages in axon formation: observations of growth of *Aplysia* axons in culture using video-enhanced contrast-differential interference contrast microscopy. J Cell Biol *103*, 1921-1931.

Goujon, M., McWilliam, H., Li, W., Valentin, F., Squizzato, S., Paern, J., and Lopez, R. (2010). A new bioinformatics analysis tools framework at EMBL-EBI. Nucleic Acids Res *38*, W695-699.

Grieder, N.C., de Cuevas, M., and Spradling, A.C. (2000). The fusome organizes the microtubule network during oocyte differentiation in *Drosophila*. Development *127*, 4253-4264.

Han, M.V., and Zmasek, C.M. (2009). phyloXML: XML for evolutionary biology and comparative genomics. BMC Bioinformatics *10*, 356.

Hancock, J.F., Cadwallader, K., Paterson, H., and Marshall, C.J. (1991). A CAAX or a CAAL motif and a second signal are sufficient for plasma membrane targeting of ras proteins. EMBO J *10*, 4033-4039.

Hassan, B.A., Bermingham, N.A., He, Y., Sun, Y., Jan, Y.N., Zoghbi, H.Y., and Bellen, H.J. (2000). *atonal* regulates neurite arborization but does not act as a proneural gene in the *Drosophila* brain. Neuron *25*, 549-561.

Heasman, J. (2006). Patterning the early Xenopus embryo. Development *133*, 1205-1217.

Helenius, J., Brouhard, G., Kalaidzidis, Y., Diez, S., and Howard, J. (2006). The depolymerizing kinesin MCAK uses lattice diffusion to rapidly target microtubule ends. Nature *441*, 115-119.

Hinrichs, M.H., Jalal, A., Brenner, B., Mandelkow, E., Kumar, S., and Scholz, T. (2012). Tau protein diffuses along the microtubule lattice. J Biol Chem *287*, 38559-38568.

Honnappa, S., Gouveia, S.M., Weisbrich, A., Damberger, F.F., Bhavesh, N.S., Jawhari, H., Grigoriev, I., van Rijssel, F.J., Buey, R.M., Lawera, A.*, et al.* (2009). An EB1-binding motif acts as a microtubule tip localization signal. Cell *138*, 366-376.

Huang, J., Zhou, W., Dong, W., Watson, A.M., and Hong, Y. (2009). From the Cover: Directed, efficient, and versatile modifications of the *Drosophila* genome by genomic engineering. Proc Natl Acad Sci U S A *106*, 8284-8289.

Kalil, K., and Dent, E.W. (2014). Branch management: mechanisms of axon branching in the developing vertebrate CNS. Nat Rev Neurosci *15*, 7-18.

Kaverina, I., Rottner, K., and Small, J.V. (1998). Targeting, capture, and stabilization of microtubules at early focal adhesions. J Cell Biol *142*, 181-190.

Kolodziej, P.A., Jan, L.Y., and Jan, Y.N. (1995). Mutations that affect the length, fasciculation, or ventral orientation of specific sensory axons in the *Drosophila* embryo. Neuron *15*, 273-286.

Krieg, M., Stühmer, J., Cueva, J.G., Fetter, R., Spilker, K., Cremers, D., Shen, K., Dunn, A.R., and Goodman, M.B. (2017). Genetic defects in β-spectrin and tau sensitize C. elegans axons to movement-induced damage via torque-tension coupling. Elife *6*, e20172.

Kumar, A., Manatschal, C., Rai, A., Grigoriev, I., Degen, M.S., Jaussi, R., Kretzschmar, I., Prota, A.E., Volkmer, R., Kammerer, R.A.*, et al.* (2017). Short Linear Sequence Motif LxxPTPh Targets Diverse Proteins to Growing Microtubule Ends. Structure *25*, 924-932 e924.

Küppers-Munther, B., Letzkus, J., Lüer, K., Technau, G., Schmidt, H., and Prokop, A. (2004). A new culturing strategy optimises *Drosophila* primary cell cultures for structural and functional analyses. Dev Biol *269*, 459-478.

Letunic, I., and Bork, P. (2018). 20 years of the SMART protein domain annotation resource. Nucleic Acids Res *46*, D493-D496.

Lewis, T.L., Jr., Courchet, J., and Polleux, F. (2013). Cell biology in neuroscience: Cellular and molecular mechanisms underlying axon formation, growth, and branching. J Cell Biol *202*, 837-848.

Luo, L., Liao, Y.J., Jan, L.Y., and Jan, Y.N. (1994). Distinct morphogenetic functions of similar small GTPases: *Drosophila* Drac1 is involved in axonal outgrowth and myoblast fusion. Genes Dev *8*, 1787-1802.

Macia, E., Partisani, M., Favard, C., Mortier, E., Zimmermann, P., Carlier, M.F., Gounon, P., Luton, F., and Franco, M. (2008). The pleckstrin homology domain of the Arf6-specific exchange factor EFA6 localizes to the plasma membrane by interacting with phosphatidylinositol 4,5-bisphosphate and F-actin. J Biol Chem *283*, 19836-19844.

Marklund, U., Larsson, N., Gradin, H.M., Brattsand, G., and Gullberg, M. (1996). Oncoprotein 18 is a phosphorylation-responsive regulator of microtubule dynamics. EMBO J *15*, 5290-5298.

McWilliam, H., Li, W., Uludag, M., Squizzato, S., Park, Y.M., Buso, N., Cowley, A.P., and Lopez, R. (2013). Analysis Tool Web Services from the EMBL-EBI. Nucleic Acids Res *41*, W597-600.

Medana, I.M., and Esiri, M.M. (2003). Axonal damage: a key predictor of outcome in human CNS diseases. Brain *126*, 515-530.

Moore, A.T., Rankin, K.E., von Dassow, G., Peris, L., Wagenbach, M., Ovechkina, Y., Andrieux, A., Job, D., and Wordeman, L. (2005). MCAK associates with the tips of polymerizing microtubules. J Cell Biol *169*, 391-397.

O'Rourke, S.M., Christensen, S.N., and Bowerman, B. (2010). *Caenorhabditis elegans* EFA-6 limits microtubule growth at the cell cortex. Nat Cell Biol *12*, 1235-1241.

Patel, J.T., Belsham, H.R., Rathbone, A.J., Wickstead, B., Gell, C., and Friel, C.T. (2016). The family-specific alpha4-helix of the kinesin-13, MCAK, is critical to microtubule end recognition. Open Biol *6*.

Paul, P., van den Hoorn, T., Jongsma, Marlieke L.M., Bakker, Mark J., Hengeveld, R., Janssen, L., Cresswell, P., Egan, David A., van Ham, M., ten Brinke, A.*, et al.* (2011). A Genome-wide Multidimensional RNAi Screen Reveals Pathways Controlling MHC Class II Antigen Presentation. Cell *145*, 268-283.

Pils, D., Horak, P., Gleiss, A., Sax, C., Fabjani, G., Moebus, V.J., Zielinski, C., Reinthaller, A., Zeillinger, R., and Krainer, M. (2005). Five genes from chromosomal band 8p22 are significantly down-regulated in ovarian carcinoma. Cancer *104*, 2417-2429.

Ponting, C.P., Phillips, C., Davies, K.E., and Blake, D.J. (1997). PDZ domains: targeting signalling molecules to sub-membranous sites. Bioessays *19*, 469-479.

Prokop, A. (2013a). The intricate relationship between microtubules and their associated motor proteins during axon growth and maintenance. Neur Dev *8*, 17.

Prokop, A. (2013b). A rough guide to *Drosophila* mating schemes. figshare, dx.doi.org/10.6084/m6089.figshare.106631.

Prokop, A. (2016). Fruit flies in biological research. Biological Sciences Review *28*, 10-14.

Prokop, A., Beaven, R., Qu, Y., and Sánchez-Soriano, N. (2013). Using fly genetics to dissect the cytoskeletal machinery of neurons during axonal growth and maintenance. J Cell Sci *126*, 2331-2341.

Prokop, A., Küppers-Munther, B., and Sánchez-Soriano, N. (2012). Using primary neuron cultures of *Drosophila* to analyse neuronal circuit formation and function. In The making and un-making of neuronal circuits in *Drosophila*, B.A. Hassan, ed. (New York, Humana Press), pp. 225-247.

Prokop, A., and Meinertzhagen, I.A. (2006). Development and structure of synaptic contacts in *Drosophila*. Semin Cell Dev Biol *17*, 20-30.

Qu, Y., Hahn, I., Webb, S.E.D., Pearce, S.P., and Prokop, A. (2017). Periodic actin structures in neuronal axons are required to maintain microtubules. Mol Biol Cell *28* 296-308.

Robinow, S., and White, K. (1991). Characterization and spatial distribution of the Elav protein during *Drosophila melanogaster* development. J Neurobiol *22*, 443-461.

Rogers, S.L., Rogers, G.C., Sharp, D.J., and Vale, R.D. (2002). *Drosophila* EB1 is important for proper assembly, dynamics, and positioning of the mitotic spindle. J Cell Biol *158*, 873-884.

Ronquist, F., Teslenko, M., van der Mark, P., Ayres, D.L., Darling, A., Hohna, S., Larget, B., Liu, L., Suchard, M.A., and Huelsenbeck, J.P. (2012). MrBayes 3.2: efficient Bayesian phylogenetic inference and model choice across a large model space. Syst Biol *61*, 539-542.

Sánchez-Soriano, N., Gonçalves-Pimentel, C., Beaven, R., Haessler, U., Ofner, L., Ballestrem, C., and Prokop, A. (2010a). *Drosophila* growth cones: a genetically tractable platform for the analysis of axonal growth dynamics. Dev Neurobiol *70*, 58-71.

Sánchez-Soriano, N., Gonçalves-Pimentel, C., Beaven, R., and Prokop, A. (2010b). Using *Drosophila* growth cones to dissect F-actin network regulation at the cellular level. Paper presented at: Actin 2009 (Bristol).

Sánchez-Soriano, N., Travis, M., Dajas-Bailador, F., Goncalves-Pimentel, C., Whitmarsh, A.J., and Prokop, A. (2009). Mouse ACF7 and *Drosophila* Short stop modulate filopodia formation and microtubule organisation during neuronal growth. Journal of cell science *122*, 2534-2542.

Schimizzi, G.V., Currie, J.D., and Rogers, S.L. (2010). Expression levels of a kinesin-13 microtubule depolymerase modulates the effectiveness of anti-microtubule agents. PLoS One *5*, e11381.

Schindelin, J., Arganda-Carreras, I., Frise, E., Kaynig, V., Longair, M., Pietzsch, T., Preibisch, S., Rueden, C., Saalfeld, S., Schmid, B.*, et al.* (2012). Fiji: an open-source platform for biological-image analysis. Nat Methods *9*, 676-682.

Seibel, N.M., Eljouni, J., Nalaskowski, M.M., and Hampe, W. (2007). Nuclear localization of enhanced green fluorescent protein homomultimers. Analytical Biochemistry *368*, 95-99.

Sharp, D.J., and Ross, J.L. (2012). Microtubule-severing enzymes at the cutting edge. Journal of cell science *125*, 2561-2569.

Sievers, F., Wilm, A., Dineen, D., Gibson, T.J., Karplus, K., Li, W., Lopez, R., McWilliam, H., Remmert, M., Soding, J.*, et al.* (2011). Fast, scalable generation of high-quality protein multiple sequence alignments using Clustal Omega. Mol Syst Biol *7*, 539.

Stefana, M.I., Driscoll, P.C., Obata, F., Pengelly, A.R., Newell, C.L., MacRae, J.I., and Gould, A.P. (2017). Developmental diet regulates *Drosophila* lifespan via lipid autotoxins. Nat Commun *8*, 1384.

Tarrade, A., Fassier, C., Courageot, S., Charvin, D., Vitte, J., Peris, L., Thorel, A., Mouisel, E., Fonknechten, N., Roblot, N.*, et al.* (2006). A mutation of spastin is responsible for swellings and impairment of transport in a region of axon characterized by changes in microtubule composition. Hum Mol Genet *15*, 3544-3558.

Tiab, L., Manzi, V.d.A., Borruat, F.-X., Munier, F., and Schorderet, D. (2004). Mutation analysis of KIF21A in congenital fibrosis of the extraocular muscles (CFEOM) patients. Ophthalmic Genetics *25*, 241-246.

Trotta, N., Orso, G., Rossetto, M.G., Daga, A., and Broadie, K. (2004). The hereditary spastic paraplegia gene, *spastin*, regulates microtubule stability to modulate synaptic structure and function. Current Biology *14*, 1135-1147.

Vale, R.D., and Toyoshima, Y.Y. (1988). Rotation and translocation of microtubules in vitro induced by dyneins from Tetrahymena cilia. Cell *52*, 459-469.

van der Vaart, B., van Riel, Wilhelmina E., Doodhi, H., Kevenaar, Josta T., Katrukha, Eugene A., Gumy, L., Bouchet, Benjamin P., Grigoriev, I., Spangler, Samantha A., Yu, Ka L.*, et al.* (2013). CFEOM1-associated kinesin KIF21A is a cortical microtubule growth inhibitor. Developmental Cell *27*, 145-160.

Voelzmann, A., Hahn, I., Pearce, S., Sánchez-Soriano, N.P., and Prokop, A. (2016a). A conceptual view at microtubule plus end dynamics in neuronal axons. Brain Res Bulletin *126*, 226-237.

Voelzmann, A., Liew, Y.-T., Qu, Y., Hahn, I., Melero, C., Sánchez-Soriano, N., and Prokop, A. (2017). *Drosophila* Short stop as a paradigm for the role and regulation of spectraplakins. Sem Cell Dev Biol *69*, 40-57.

Voelzmann, A., Okenve-Ramos, P., Qu, Y., Chojnowska-Monga, M., del Caño-Espinel, M., Prokop, A., and Sánchez-Soriano, N. (2016b). Tau and spectraplakins promote synapse formation and maintenance through Jun kinase and neuronal trafficking. eLife *5*, e14694.

Wang, J.T., Medress, Z.A., and Barres, B.A. (2012). Axon degeneration: molecular mechanisms of a self-destruction pathway. J Cell Biol *196*, 7-18.

Yu, W., Qiang, L., Solowska, J.M., Karabay, A., Korulu, S., and Baas, P.W. (2008). The microtubule-severing proteins spastin and katanin participate differently in the formation of axonal branches. Mol Biol Cell *19*, 1485-1498.

Zeidler, M.P., Tan, C., Bellaiche, Y., Cherry, S., Hader, S., Gayko, U., and Perrimon, N. (2004). Temperature-sensitive control of protein activity by conditionally splicing inteins. Nat Biotech *22*, 871-876.

Zhang, D., Grode, K.D., Stewman, S.F., Diaz-Valencia, J.D., Liebling, E., Rath, U., Riera, T., Currie, J.D., Buster, D.W., Asenjo, A.B.*, et al.* (2011). *Drosophila* katanin is a microtubule depolymerase that regulates cortical-microtubule plus-end interactions and cell migration. Nat Cell Biol *13*, 361-370.

Zschätzsch, M., Oliva, C., Langen, M., De Geest, N., Ozel, M.N., Williamson, W.R., Lemon, W.C., Soldano, A., Munck, S., Hiesinger, P.R.*, et al.* (2014). Regulation of branching dynamics by axon-intrinsic asymmetries in Tyrosine Kinase Receptor signaling. Elife *3*, e01699.

Figures

Fig. 1 Efa6 is expressed throughout neurons at all developmental stages

A-E) Images of primary *Drosophila* neurons at 6HIV or 5DIV (at indicated bottom right), stained for tubulin (magenta) and GFP (green); control neurons are wild-type (wt) or express *elav-Gal4*-driven nuclear GFP (*elav / nl-GFP*), whereas further neurons are either derived from the endogenously tagged Efa6::GFP line or express Efa6-FL::GFP under the control of sca-Gal4 (*sca / Efa6-FL::GFP*); asterisks indicate cell bodies and arrow the axon tips. F-I) Late larval CNSs at about 4d of development from egg lay (L3; F,G) and adult CNSs at over 10d of development (H,I) derived from control wild-type animals (wt) or the Efa6::GFP line (*Efa6::GFP*), stained for GFP and actin (Phalloidin, only larval preparations); OL, optic lobe; Br, central brain; vNC, ventral nerve cord. Scale bar in A represent 15µm in A-C, 25µm in D and E, 75µm in F and G, 130µm in H and I.

Fig. 2. Efa6 regulates axonal length and branch numbers in primary *Drosophila* neurons. Examples of primary *Drosophila* neurons at 6HIV (A-C) or at 5DIV (E-H), all stained for actin (magenta) and tubulin (green); neurons are either wild-type controls (A, E), Efa6-deficient (B, F), expressing Efa6-FL::GFP (C, G), or expressing Efa6-Nterm-CAAX::GFP (H); asterisks indicate cell bodies, arrows point at axon tips, arrow heads at axon branches, the curved arrow at an area of MT disorganisation; the scale bar in G represents 10µm in A-C and 20µm in E-H. Quantification of axon lengths at 6HIV (D) and of axonal branch numbers (I); different genotypes are colour-coded: grey, wild-type controls; blue, different *Efa6* loss-of-function conditions; green, neurons over-expressing Efa6 variants; data represent fold-change relative to wild-type controls (indicated as horizontal dashed "ctrl" line); they are shown as single data points and a bar indicating mean ± SEM data; P values from Mann-Whitney tests are given above each column, sample numbers at the bottom of each bar.

Fig. 3. Efa6 regulates axon branching in the adult fly brain. A-F) Brains (medulla region of the optic lobe in oblique view) of young (2-5 d after eclosure; top) and old flies (15-18 d; bottom) driving *UAS-myr-tdTomato* via the *ato-Gal4* driver in dorsal cluster neurons (example neurons are traced in magenta for axons and green for side branches); flies are either wild-type controls (left) or display *ato-Gal4*-driven knock-down of Efa6 (middle) or over-expression of Efa6-FL::GFP (right). G,H) Quantification of data for wild-type (wt; grey), Efa6 knock-down (blue) and Efa6-FL::GFP over-expression (green), displaying the number of primary branches per axon (G), all representing fold-change relative to wild-type controls (indicated as horizontal dashed "ctrl" line); data are shown as bars indicating mean ± SEM in G accompanied by single data point and binary score normalised to wt in H.; P values from Mann-Whitney or Chi^2 tests are respectively given above each column, sample numbers at the bottom of each bar (in G number of medullas before and number of axons after slash). Scale bar in D represents 60µm in all figures.

Fig. 4. Efa6 helps to maintain axonal MT bundles in *Drosophila* neurons. A-H) Images of primary neurons at 6HIV (left), 5DIV (middle) and 10DIV (right), stained for tubulin (green) and actin (magenta), derived from embryos that were either wildtype (wt, A-C), *Efa6* null mutant (D-F), homozygous for $shot^3$ (G) or $shot^3$ $Efa6^{GX6[w-]}$ double-mutant (shot Efa6) (H); arrows

point at axon tip, arrow heads at areas of MT disorganisation, and asterisks indicate the cell bodies; the scale bar in A represents 10µm for 6HIV neurons and 25µm for 5DIV and 10DIV neurons. I-M) Quantitative analyses of MT disorganisation (measured as MT disorganisation index, MDI) in different experimental contexts (as indicated above graphs); different genotypes are colour-coded: grey, wild-type controls; blue, *Efa6* loss-of-function; light/dark orange, *shot*^{3} in hetero-/homozygosis; green, neurons over-expressing Efa-FL::GFP; data are shown as single data points and a bar indicating mean ± SEM, all representing fold-change relative to wild-type controls (indicated as horizontal dashed "ctrl" line); P values from Mann-Whitney tests in I, J) and Kruskal–Wallis one-way ANOVA with *post hoc* Dunn's test in K-M) are given above each column, sample numbers at the bottom of each bar.

Fig. 5 Efa6 is required for axonal MT bundle maintenance in adult fly brains. A-C) Medulla region of adult brains at 26-27 days after eclosure, all carrying the *GMR31F10-Gal4* driver and *UAS-α-tubulin84B-GFP* (*GMR-tub*) which together stain MTs in a subset of lamina neuron axons that terminate in the medulla; the other specimens co-express *Efa6-RNAi* either alone (*GMR-tub-Efa6*^{IR} in B) or combined with a *shot*$^{3/+}$ heterozygous mutant background (*GMR-tub-Efa6*^{IR} *shot*$^{3/+}$ in C); white/black arrows indicate axonal swellings without/with MT disorganisation; rectangles outlined by red dashed lines are shown as 2.5 fold magnified insets where white arrow heads point at disorganised MTs; the scale bar in A represents 15µm in all images. D, E) Quantitative analyses of all axonal swelling (D) or swellings with MT disorganisation (E); different genotypes are colour-coded as indicated; bars show mean ± SEM, all representing fold-change relative to wild-type controls (indicated as horizontal dashed line); P values from Kruskal–Wallis one-way tests are given above each column, sample numbers at the bottom of each bar.

Fig. 6. Efa6 regulates MT behaviours in GCs. A-H') Examples of primary neurons at 6HIV which are either wild-type controls (top), Efa6-deficient (middle) or expressing Efa6-FL::GFP (bottom); neurons were either imaged live for Eb1::GFP (green in A,D) or fixed and labelled for Eb1 and tubulin (B,E,G; as colour-coded) or actin and tubulin (C,F,H; as colour coded; tubulin shown as single channel image on the right); asterisks indicate cell bodies, white arrows the tips of GCs, open arrows the tips of MT bundles and arrow heads MTs or Eb1 comets in filopodial processes; the GC in G is outlined with a white dashed line; scale bar in D represents 5µm in all images. I-M) Quantitative analyses of MT behaviours in GCs of such neurons as indicated above each graph (for axon shaft analyses see Fig.7). Different genotypes are colour-coded: grey, wild-type controls; blue, different *Efa6* loss-of-function conditions; green, neurons over-expressing Efa-FL; data are shown as single data points and a bar indicating mean ± SEM, all representing fold-increase relative to wild-type controls (indicated as horizontal dashed "ctrl" line); P values from Mann-Whitney tests are given above each column, sample numbers at the bottom of each bar. The graph in L shows percentages of neurons with (light shade) or without (dark shade) any MTs in GC filopodia; numbers above bars indicate P values from Chi^{2} tests. Throughout the figure, data obtained from live analyses with Eb1::GFP are framed in red.

Fig. 7. Loss of Efa6 promotes MT entry into shaft filopodia. Quantitative analyses of MT behaviours in axon shafts, as indicated above each graph; bars are colour-coded: grey, controls; blue, different *Efa6* mutant alleles; green, neurons over-expressing Efa-FL::GFP; red

outlines indicate live imaging data, all others were obtained from fixed specimens. A-C,G,H) data all represent fold-change relative to wild-type controls (indicated as horizontal dashed "ctrl" line) and are shown as single data points and a bar indicating mean ± SEM; P values from Mann-Whitney tests are given above each column, sample numbers at the bottom of each bar. D-F) Percentages of antero- / retrograde comet movements (D), percentage of neurons harbouring at least one filopodium containing / lacking Eb1 comets (E) or containing / lacking tubulin-stained MTs (F); fractions indicated by light / dark shades as indicated; G) number of tubulin-stained MTs in shaft filopodia relative to axon length normalised to wildtype controls; H) number of axon shaft filopodia containing MTs (values relative to ctrl); numbers on top or at the upper limit of the bars indicate P values from Chi^2 tests.

Fig. 8. Efa6 domain and motif requirements for MT elimination in neurons and fibroblasts. A) Schematics of *Drosophila melanogaster (Dm)* Efa6 (isoform C, CG31158), *Caenorhabditis elegans (Ce)* Efa6 (isoform Y55D9A.1a) and *Homo sapiens* (human) PSD(1) (isoform 201/202, NP_002770.3), illustrating the positions (numbers indicate first and last residues) of the putative PSD95-Dlg1-ZO1 domain (PDZ), SxIP/SxLP motifs (SRIP, SQIP, SALP, SSLP), the MT-binding domain (MTED), SEC7 domain, plekstrin homology (PH) domain and coiled-coil domain (CC). B) Schematics on the left follow the same colour code and show the *D.m.* Efa6 constructs used in this study (dashed red lines indicate the last/first residue before/behind the truncation). Bar graphs on the right show the impact that transfection of these constructs had on axon loss in primary *Drosophila* neurons (dark grey in left graph) and on MT loss in fibroblasts (dark grey or black as indicated); for respective images see F and G and Fig.S9) Analogous fibroblast experiments as performed with *Drosophila* constructs were performed with full length constructs of *C. elegans* Efa6 and human PSDs (C), with N-terminal constructs (D) or synthetic MTEDs (E) of *Dm* and *Ce*Efa6 and of human PSD(1). Throughout this figure, construct names are highlighted in red for *Drosophila*, light blue for *C. elegans* and yellow for *Homo sapiens*; all graph bars indicate percentages of neurons with/without axons (light/dark grey) and of fibroblasts with normal, reduced or absent MTs (light, medium, dark grey, respectively); numbers in the left end of each bar indicate sample numbers, on the right end the P values from Chi^2 tests relative to GFP controls; numbers on the right of bars in B compare some constructs to Efa6-FL::GFP, as indicated by black lines. For raw data see T8 Primary neurons expressing Efa6-FL::GFP transgenically and stained for tubulin (asterisks, cell bodies; white arrows, axon tips; open arrow, absent axon). G-G") Fibroblasts expressing Efa6-FL::GFP and stained for tubulin; curved arrows indicate areas where MTs are retracted from the cell periphery; grey dots in F-G" indicate the phenotypic categories for each neuron and fibroblasts, as used for quantitative analyses in the graphs above. Scale bar at bottom of F refers to 10µm in F and 25µm in G.

Fig. 9. A model of the suggested roles of Efa6. **A**) The model of local axon homeostasis (Prokop, 2016; Voelzmann et al., 2016a) states that axonal MTs (green bars) are actively kept in bundles; for example, their continued polymerisation (1) mediated by plus end machinery (blue circle) is guided by spectraplakins (here Shot) along cortical actin into parallel bundles (2), or MTs are kept together through cross-linkage (brown “L”; 4) (Bettencourt da Cruz et al., 2005; Krieg et al., 2017); here we propose that MTs accidentally leaving the bundle become vulnerable (orange circles) through elimination (red “T”) by cortically anchored Efa6. **B**) In normal neurons, polymerising MTs in bundles (dark blue circles) are protected by Shot (marine lines) and MT-MT cross-linkers (brown rectangles), whereas MTs approaches the

membrane (orange arrow heads) either by splaying out in GCs or leaving the bundle in the shaft (orange arrow heads) become vulnerable (orange circles) to elimination by Efa6 (light green/red dashes) both along the cortex and in filopodia **C**) Upon Efa6 deficiency, MTs leaving bundles or entering GCs are no longer subjected to Efa6-mediated cortical elimination (blue arrow heads) and can cause gradual build-up of MT disorganisation; when entering shaft filopodia they can promote interstitial branch formation (red arrow), when entering GC filopodia they can promote axon growth or even branching through GC splitting (yellow arrows). **D**) Far more MTs leave the bundles in *shot* mutant neurons, but a good fraction of them is eliminated by Efa6 (increased number of orange arrow heads). **E**) In the absence of both Shot and Efa6, more MTs leave the bundles, but there is no compensating cortical elimination (increased number of blue arrow heads), so that the MT disorganisation phenotype worsens**.**

Supplementary materials

Fig.S1 *ato-Gal4*-driven Efa-FL::GFP expression in adult brains. Brains (region of the optic lobe in oblique view; white dashed line indicating the lower edge of the medulla) of young (2-5 d after eclosure; top) and old flies (15-18 d; bottom) which are either from wild-type controls or from flies driving *UAS-myr-tdTomato* and *UAS-Efa6-FL-GFP* via the *ato-Gal4* driver in dorsal cluster neurons; specimens are stained for GFP and arrows point at stained; for myr-dtTomato staining of brains from these experiments see Fig. 3. Scale bar in D represents 60µm in all images.

Fig. S2. Efa6 mutant primary neurons show MT disorganisation. Quantitative analyses of MT disorganisation measured as binary score (percentage of neurons showing obvious MT disorganisation in their axons) in different *Efa6* mutant alleles (control value indicated as horizontal dashed "ctrl" line); P values from Chi^2 tests are given above the bars.

Fig. S3 Phylogentic tree analysis of Efa6. Bayesian phylogenetic analysis of full length (A) or N-termini (B) of Efa6 orthologues. Sequences were aligned using Muscle or ClustalO and posterior probabilities and branch lengths calculated using MrBayes. Branch length scale is indicated; blue numbers show posterior probabilities of each branch split. For the full length tree, *Drosophila steppke* (*step*) was used as outgroup. In both full length and N-terminus analyses, chordates (cream colour) split off very early from Efa6 versions of other species, in line with an early speciation event separating both groups before the vertebrate multiplication events took place. Phyla are highlighted in different colours, gene symbols and/or accession numbers are given after the species names.

Fig. S4. Efa6 N-terminal domains vary amongst different phyla. A) Domain annotations in 56 Efa6 orthologues via EMBL SMART and Uniprot. Phyla are colour-coded as in Fig.S3. Note that there is a strong variation of lengths and domain composition in particular of the N-terminus. The putative PDZ domain is not present in any analysed chordate orthologue, and MTED and MTED-like sequences cannot be consistently identified in all Efa6 orthologues and are very divergent in chordate Efa6/Psd versions. Only a subset of nematode (e.g. *C.*

elegans) and insect (e.g. *D. melanogaster*) Efa6 versions, and even fewer chordate Efa6/PSD proteins, contain SxIP/SxLP sites flanked by positive charges (as would be expected of functional sites) (Honnappa et al., 2009) in the N-terminal half of the protein; in mouse, alpaca and cat SxIP/SxLP sites are flanked by negative charges. B) To determine a potential MTED consensus sequence, 37 sequences of molluscs, nematodes, arthropods and putative MTED sequences of mammalian PSD1-4 were grouped according to phylum; consensus sequences were depicted using Berkley's Weblogo online server (default colour scheme). Conserved amino acid positions are highlighted (faint yellow).

Fig.S5. Localisation of Efa6 constructs in primary neurons. Images show transfected primary *Drosophila* neurons at 18HIV stained for tubulin (magenta) and GFP (green and in greyscale below the colour image). Cell bodies are indicated by asterisks, axon tips by arrows. The transfected constructs are indicated top right following the nomenclature explained in Fig.8. Scale bar in A represents 10µm for all figures shown.

Fig.S6. Efa6 constructs localisations in fibroblasts. Images show fibroblasts which are all stained for GFP (green) and either for actin or MTs (magenta); GFP and actin/MTs shown as single channels in greyscale below the colour image, 24hrs after transfection with control (GFP) or Efa6-derived constructs (nomenclature as explained in Fig.8, but leaving out the "Efa6"-prefix and "::GFP"-postfix, as indicated top right. Double chevrons indicate nuclear localisation, arrow heads membrane localisation apparent at cell edges and curved arrows membrane ruffles. Scale bar in A represents 10µm in all images.

Fig.S7. MT elimination by Efa6-FL is concentration-dependent in fibroblasts. A-C) Representative images of fibroblasts stained for GFP and tubulin (green and magenta, respectively; both shown as single channels in greyscale below the colour image). Images were taken 24hrs after transfection with *Efa6-FL::GFP*, assessed for GFP intensity (plotted on the ordinate in D; examples for low, moderate and high expression are given in the left, middle and right columns, respectively) and then grouped with respect to their MT phenotypes into "MTs intact" (light grey), "mild MT defects" (medium grey) or "MTs gone" (black), as indicated by greyscale circles in the lowest row of A-C and the abscissa of D. Arrow heads point at GFP accumulation at membrane edges, white arrows indicate areas of the cell from where MTs have retracted, open arrows point at retraction fibres and the double chevron indicates the nucleus position and signs of nuclear GFP localisation. Scale bar in A represents 10µm in all images.

Fig. S8. Conserved functions of the Efa6 C-terminus in membrane ruffle formation. A-E) Representative images of fibroblasts stained for GFP and actin (green and magenta, respectively; both shown as single channels in greyscale below the colour image). Images were taken 24hrs after transfection with different constructs (indicated top right): control vector (GFP; A), Efa6-derived constructs (B-D; nomenclature as explained in Fig.8, but leaving out the "Efa6"-prefix and "::GFP"-postfix) or PSD(1)-FL::GFP (E). To the right of each image, a selected area is displayed with 2.5-fold magnification, showing dotted actin- and GFP-stained ruffles in B, D and E, but not A and C; ruffle formation has been quantified and is shown as a bar graph in F. All graph bars indicate percentages of fibroblasts with/without membrane

ruffles (dark/light grey); P values on top of bars are from Chi^2 tests relative to GFP controls;. Scale bar in the top image of A represents 10 µM for all fibroblasts shown.

Fig.S9. Representative MT phenotypes induced by the different constructs in transfected fibroblasts. Fibroblasts 24hrs after transfection with different control (GFP) or Efa6-derived constructs as indicated top right in each image (nomenclature as explained in Fig.8, but leaving out the "Efa6"-prefix and "::GFP"-postfix). Cells were stained for tubulin (black; images shown as inverted greyscale) and classified as "no MT defects" (light grey), "mild MT defects" (medium grey) or "MTs gone" (black), as indicated by greyscale boxes bottom left of each image. Each image represents the most prominent phenotype for each respective construct. Scale bar at the bottom right in H represents 25µm in all images.

Fig. S10. *In vitro* attempts to resolve the MT elimination mechanism of Efa6. A) To determine whether Efa6 directly affects MT stability, we recombinantly expressed Efa6-ΔCterm::GFP in Sf9 cells, purified the protein and observed its interaction with MTs using total internal reflection fluorescence (TIRF) microscopy in a low ionic strength buffer (BRB20, 75mM KCl); images on the left show three examples of kymographs of MT lattices decorated with Efa6-ΔCterm::GFP, which displays a mixture of stationary molecules and diffusive interactions typical of non-translocating MT-associated proteins (Helenius et al., 2006; Hinrichs et al., 2012); bar charts (right) show quantification of the amount of interacting protein: background signal from MTs alone, Efa6-ΔCterm::GFP (20nM) and the non-translocating kinesin MCAK::GFP (20nM) as positive control; at the same protein concentration, over 2-fold more molecules of MKAC typically interact with MTs; all graphs in this figure show individual data points and bars representing mean ± SEM; numbers above bars show P values obtained from Mann–Whitney Rank Sum statistical analyses, numbers in bars the respective sample numbers. B) Kymographs (left) show individual fluorescently-labelled GMPCPP-stabilised MTs *in vitro* (Patel et al., 2016), either alone (MTs only; basal depolymerisation rate, n=7) or in the presence of 14 nM Efa6-ΔCterm::GFP (n=8) or 40nM MCAK::GFP (n=18); the bar chart (right) quantifies the induced depolymerisation rates; using two different purifications of Efa6-ΔCterm::GFP on three separate occasions, we saw no evidence of MT depolymerisation above the basal level of depolymerisation typically observed in these assays, whereas parallel control experiments with mitotic centromere-associated kinesin/MCAK showed MT depolymerisation rates typical of this kinesin. C) To assess whether MT destabilisation might require additional cytoplasmic factors, we used *Xenopus* oocyte extracts: phase contrast images show MTs in *Xenopus* oocyte extracts (after they had been allowed to polymerise for 20 min) and then showing stills from before, 10s after and 120s after washing in 20nM MCAK::GFP (as positive control), 20nM Efa6-ΔCterm::GFP or 40nM synthetic MTED (to overcome potential mis-folding of the purified ΔCterm protein); squares outlined by dashed white lines are shown magnified in insets revealing MTs; MTs clearly vanish upon treatment with MCAK, but counts of MTs did not reveal any obvious effects on MTs with either of the Efa6 peptides. D) Finally, interference with MT polymerisation was analysed by adding 20nM MTED to diluted *Xenopus* cytosol, and 20 random fields were recorded 10 min later via VE-DIC microscopy and the numbers of MTs per field counted; data plots show that MTED does not interfere with MT polymerisation. E,F) *RFP* controls and *Efa6-Nterm::GFP* expression constructs were injected into *Xenopus* embryos at the 4-cell stage and analysed 24 hrs later; only the *Efa6* construct caused a strong suppression of cell division, as indicated by the presence of very large cells (arrows) and pigmentation defects (curved arrows) at the site of

injection, suggesting that Efa6-Nterm::GFP is functional when expressed in the *Xenopus* context. Taken together, the very different data obtained in *Xenopus* cytosol *in vitro* or embryos *in vivo*, suggest that either the effect of Efa6 requires a factor absent from Xenopus extract or that Efa6-ΔCterm::GFP and MTED are non-functional due to mis-folding. The latter is suggested by the observation of many aggregates of Efa6-ΔCterm::GFP in A. Scale bar (in top left image) represents 3 µm in C (2.5 fold magnified insets), and 1400 µm / 350 µm / 140 µm in left / middle / right images of E and F, respectively.

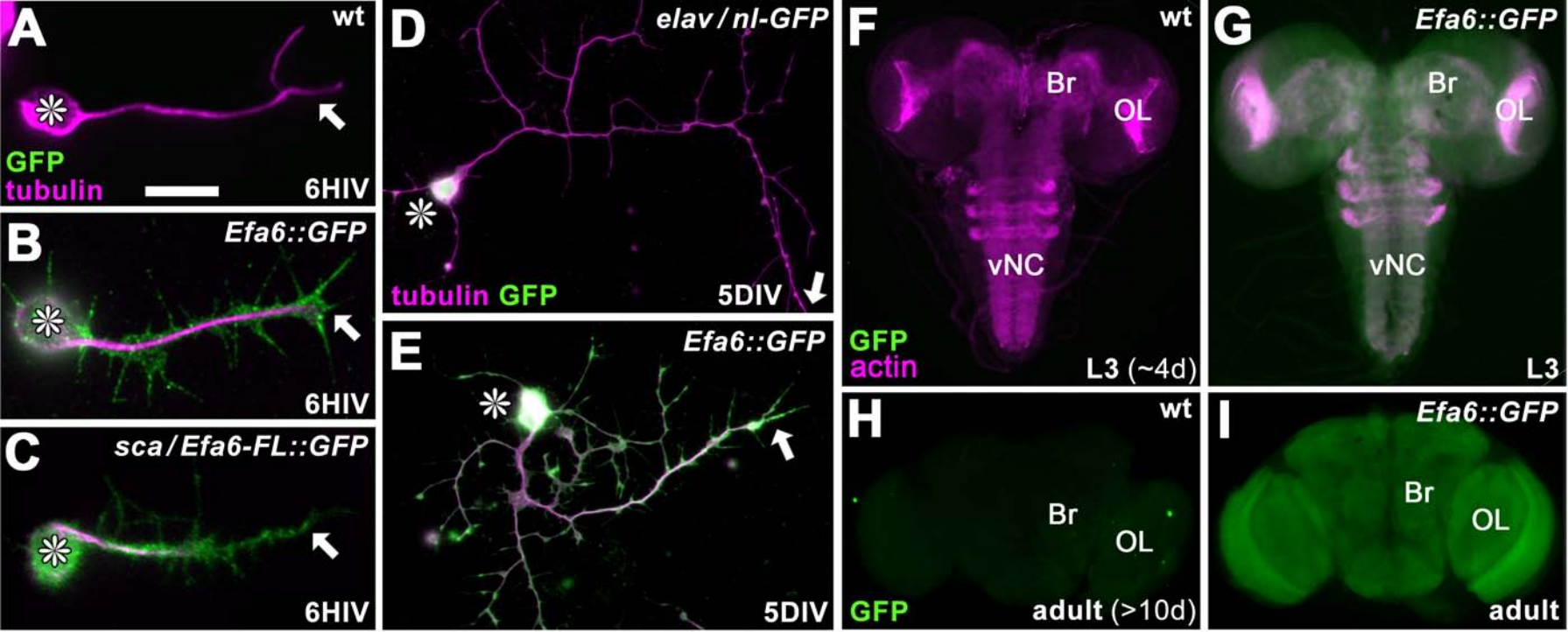
A
wt
GFP
tubulin
6HIV
B
Efa6::GFP
6HIV
C
sca/Efa6-FL::GFP
6HIV
D
elav/nl-GFP
tubulin GFP
5DIV
E
Efa6::GFP
5DIV
F
wt
Br
OL
vNC
GFP
actin
L3 (~4d)
G
Efa6::GFP
Br
OL
vNC
L3
H
wt
Br
OL
GFP
adult (>10d)
I
Efa6::GFP
Br
OL
adult

Fig.1 Qu et al.

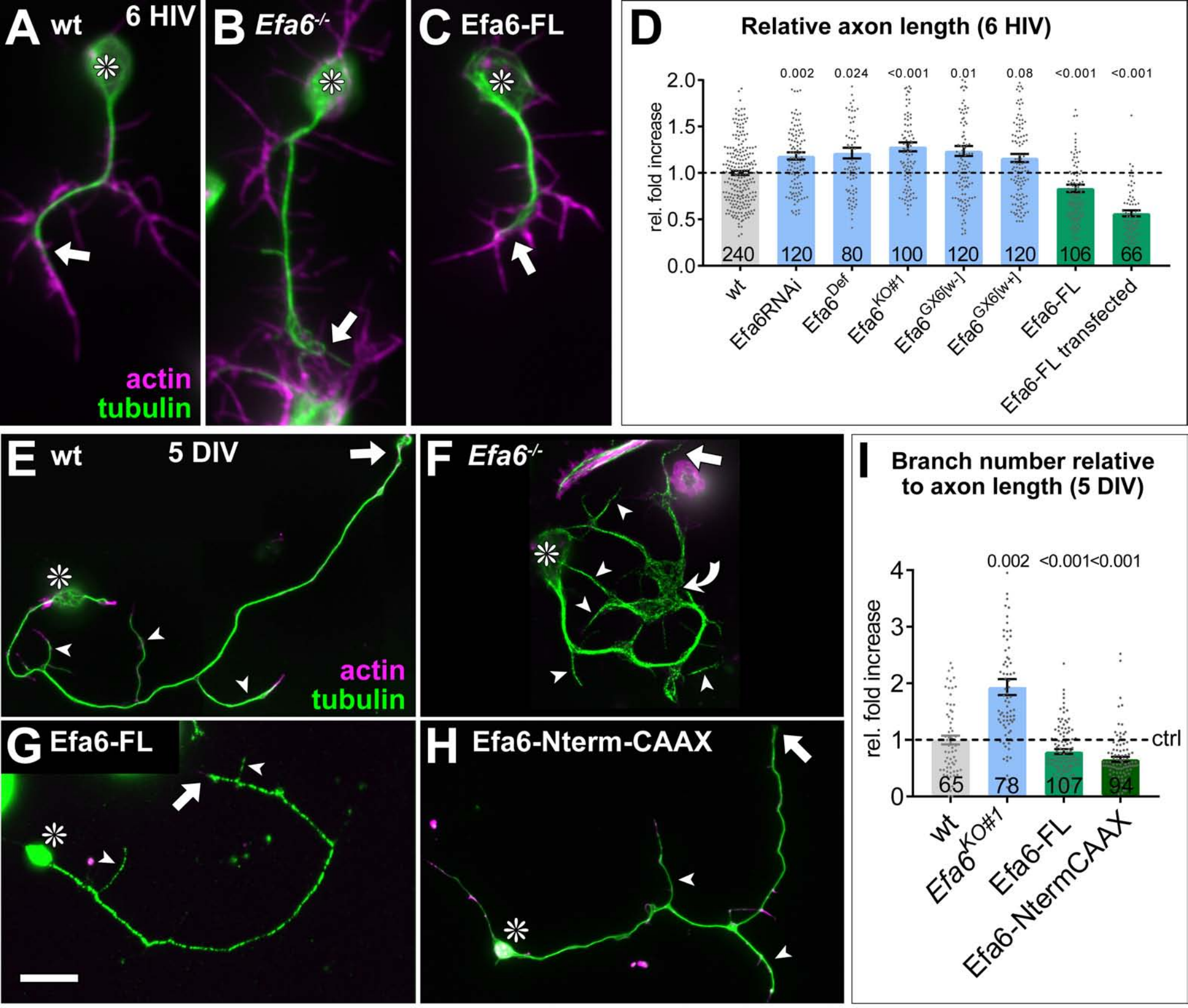
A wt
6 HIV
actin
tubulin
B Efa6-/-
C Efa6-FL
D
Relative axon length (6 HIV)
rel. fold increase
2.0
1.5
1.0
0.5
0.0
0.002
0.024
<0.001
0.01
0.08
<0.001
<0.001
240
120
80
100
120
120
106
66
wt
Efa6RNAi
Efa6Def
Efa6KO#1
Efa6GX6[w-]
Efa6GX6[w+]
Efa6-FL
Efa6-FL transfected
E wt
5 DIV
actin
tubulin
F Efa6-/-
G Efa6-FL
H Efa6-Nterm-CAAX
I
Branch number relative to axon length (5 DIV)
rel. fold increase
4
3
2
1
0
0.002
<0.001
<0.001
ctrl
65
78
107
94
wt
Efa6KO#1
Efa6-FL
Efa6-NtermCAAX

Fig. 2 Qu et al.

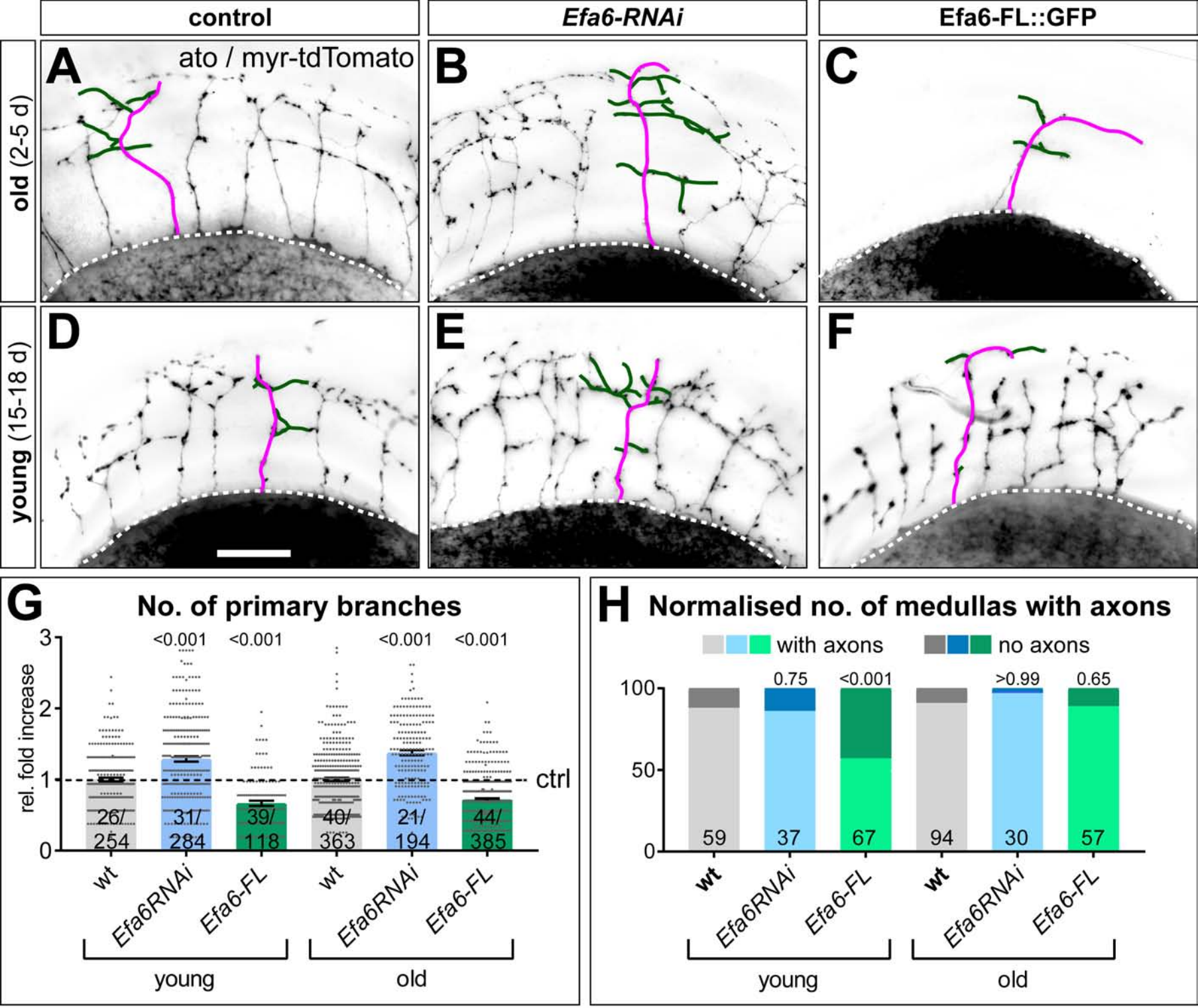
control
Efa6-RNAi
Efa6-FL::GFP
old (2-5 d)
young (15-18 d)
A
ato / myr-tdTomato
B
C
D
E
F
G
No. of primary branches
rel. fold increase
ctrl
<0.001
<0.001
<0.001
<0.001
26/ 254
31/ 284
39/ 118
40/ 363
21/ 194
44/ 385
wt
Efa6RNAi
Efa6-FL
young
old
H
Normalised no. of medullas with axons
with axons
no axons
0.75
<0.001
>0.99
0.65
59
37
67
94
30
57
wt
Efa6RNAi
Efa6-FL
young
old

Fig. 3 Qu et al.

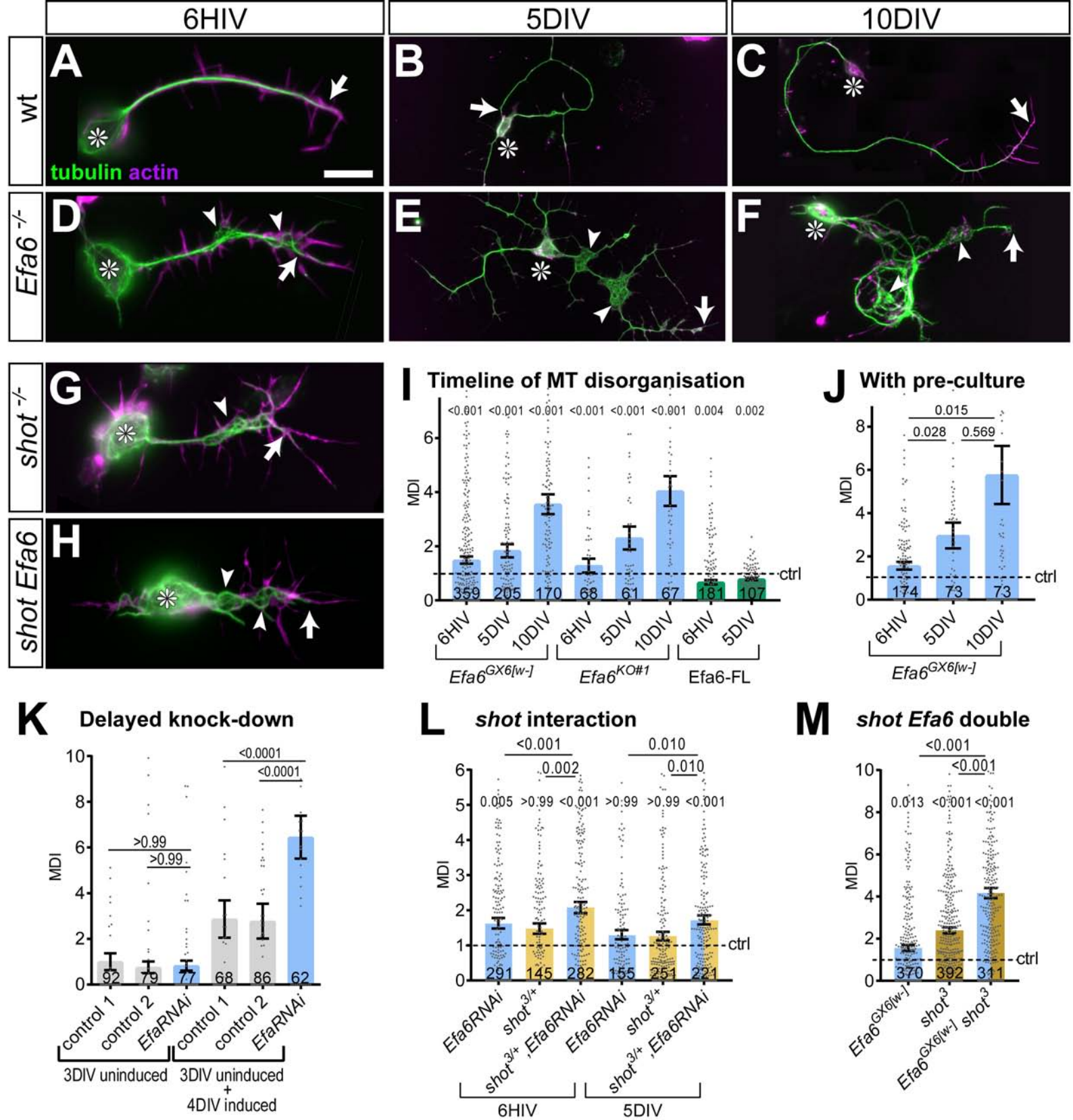
6HIV
5DIV
10DIV
wt
Efa6 -/-
shot -/-
shot Efa6
A
B
C
D
E
F
G
H
tubulin actin
I Timeline of MT disorganisation
MDI
ctrl
<0.001 <0.001 <0.001 <0.001 <0.001 <0.001 0.004 0.002
359 205 170 68 61 67 181 107
6HIV 5DIV 10DIV 6HIV 5DIV 10DIV 6HIV 5DIV
Efa6GX6[w-]
Efa6KO#1
Efa6-FL
J With pre-culture
0.015
0.028 0.569
174 73 73
6HIV 5DIV 10DIV
Efa6GX6[w-]
K Delayed knock-down
<0.0001
<0.0001
>0.99
>0.99
92 79 77 68 86 62
control 1 control 2 EfaRNAi control 1 control 2 EfaRNAi
3DIV uninduced
3DIV uninduced + 4DIV induced
L shot interaction
<0.001
0.002
0.010
0.010
0.005 >0.99 <0.001 >0.99 >0.99 <0.001
291 145 282 155 251 221
Efa6RNAi
shot3/+
shot3/+,Efa6RNAi
6HIV
5DIV
M shot Efa6 double
<0.001
<0.001
0.013 <0.001 <0.001
370 392 311
Efa6GX6[w-]
shot3
Efa6GX6[w-] shot3

Fig. 4 Qu et al.

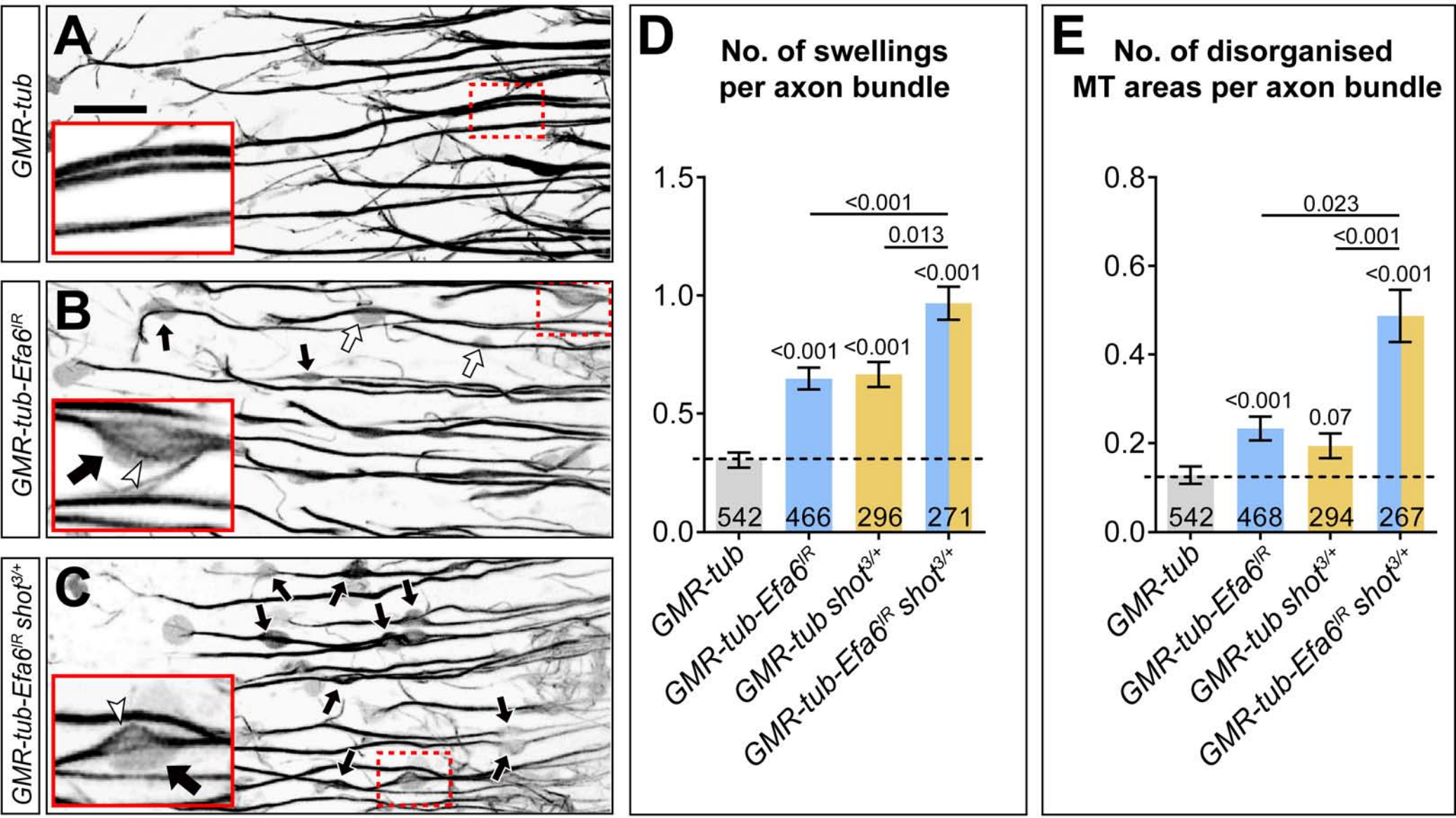
A
GMR-tub
B
GMR-tub-Efa6IR
C
GMR-tub-Efa6IR shot3/+
D
No. of swellings per axon bundle
1.5
1.0
0.5
0.0
<0.001
0.013
<0.001
<0.001
<0.001
542
466
296
271
GMR-tub
GMR-tub-Efa6IR
GMR-tub shot3/+
GMR-tub-Efa6IR shot3/+
E
No. of disorganised MT areas per axon bundle
0.8
0.6
0.4
0.2
0.0
0.023
<0.001
<0.001
0.07
<0.001
542
468
294
267
GMR-tub
GMR-tub-Efa6IR
GMR-tub shot3/+
GMR-tub-Efa6IR shot3/+

Fig. 5 Qu et al.

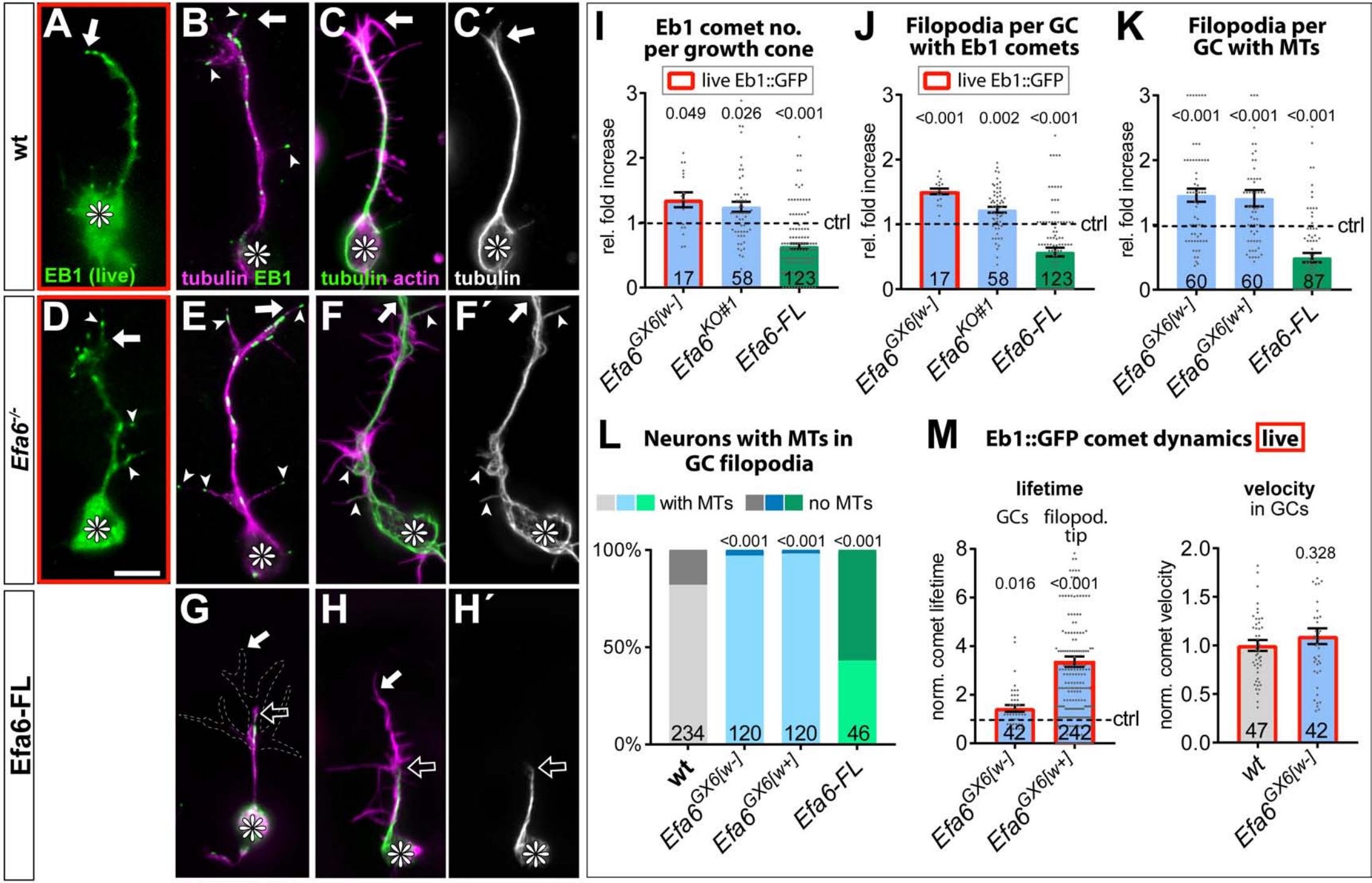
wt
Efa6-/-
Efa6-FL
A
B
C
C´
D
E
F
F´
G
H
H´
EB1 (live)
tubulin EB1
tubulin actin
tubulin
I
Eb1 comet no. per growth cone
live Eb1::GFP
rel. fold increase
ctrl
0.049
0.026
<0.001
17
58
123
Efa6GX6[w-]
Efa6KO#1
Efa6-FL
J
Filopodia per GC with Eb1 comets
live Eb1::GFP
<0.001
0.002
<0.001
17
58
123
K
Filopodia per GC with MTs
<0.001
<0.001
<0.001
60
60
87
Efa6GX6[w+]
L
Neurons with MTs in GC filopodia
with MTs
no MTs
100%
50%
0%
<0.001
<0.001
<0.001
234
120
120
46
wt
M
Eb1::GFP comet dynamics live
lifetime
GCs
filopod. tip
norm. comet lifetime
0.016
<0.001
42
242
velocity in GCs
norm. comet velocity
0.328
47
42

Fig. 6 Qu et al.

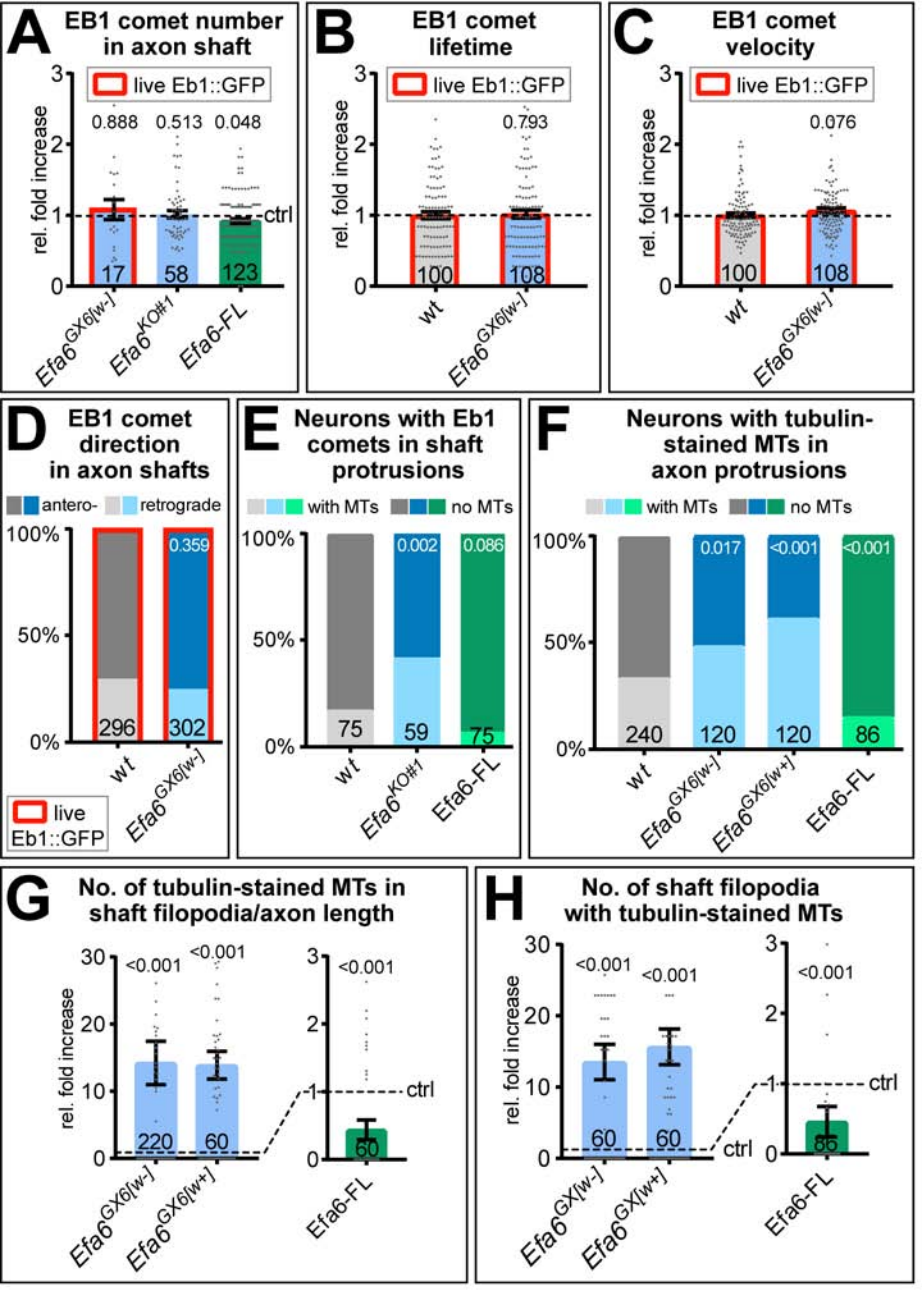
A
EB1 comet number in axon shaft
live Eb1::GFP
0.888
0.513
0.048
rel. fold increase
ctrl
17
58
123
Efa6GX6[w-]
Efa6KO#1
Efa6-FL
B
EB1 comet lifetime
live Eb1::GFP
0.793
100
108
wt
Efa6GX6[w-]
C
EB1 comet velocity
live Eb1::GFP
0.076
100
108
D
EB1 comet direction in axon shafts
antero-
retrograde
100%
50%
0%
0.359
296
302
live Eb1::GFP
E
Neurons with Eb1 comets in shaft protrusions
with MTs
no MTs
0.002
0.086
75
59
75
F
Neurons with tubulin-stained MTs in axon protrusions
0.017
<0.001
<0.001
240
120
120
86
Efa6GX6[w+]
G
No. of tubulin-stained MTs in shaft filopodia/axon length
<0.001
220
60
H
No. of shaft filopodia with tubulin-stained MTs
60
60
85

Fig. 7 Qu et al.

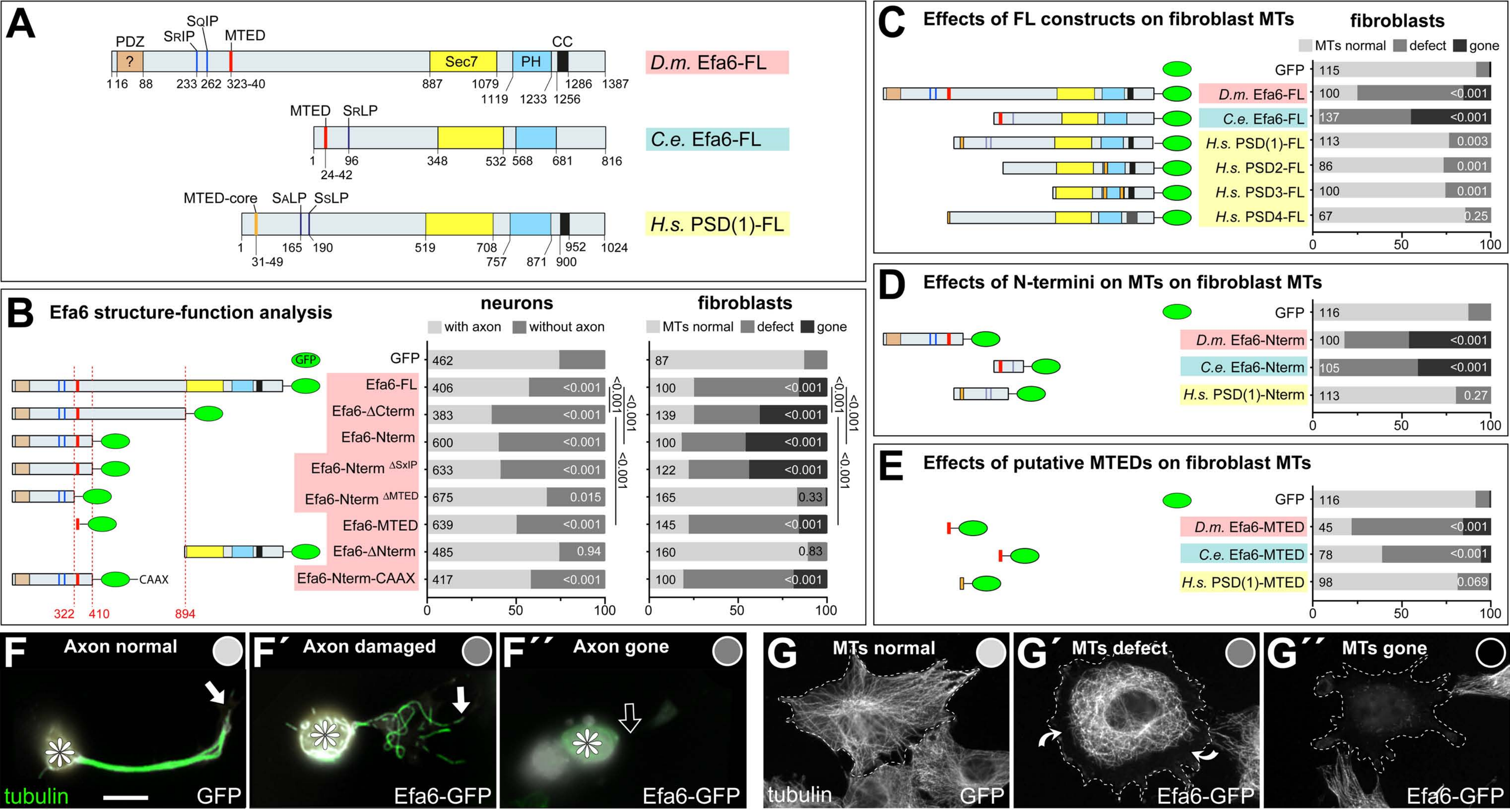
A
PDZ
SRIP
SQIP
MTED
CC
?
Sec7
PH
D.m. Efa6-FL
1 16 88 233 262 323-40 887 1079 1119 1233 1256 1286 1387
MTED SRLP
C.e. Efa6-FL
1 96 24-42 348 532 568 681 816
MTED-core SALP SSLP
H.s. PSD(1)-FL
1 165 190 31-49 519 708 757 871 900 952 1024
B
Efa6 structure-function analysis
neurons
with axon without axon
fibroblasts
MTs normal defect gone
GFP
Efa6-FL
Efa6-ΔCterm
Efa6-Nterm
Efa6-Nterm ΔSxIP
Efa6-Nterm ΔMTED
Efa6-MTED
Efa6-ΔNterm
Efa6-Nterm-CAAX
CAAX
322 410 894
462 <0.001
406 <0.001
383 <0.001
600 <0.001
633 <0.001
675 0.015
639 <0.001
485 0.94
417 <0.001
87 <0.001
100 <0.001
139 <0.001
100 <0.001
122 <0.001
165 0.33
145 <0.001
160 0.83
100 <0.001
<0.001
0 50 100
C
Effects of FL constructs on fibroblast MTs
GFP 115
D.m. Efa6-FL 100 <0.001
C.e. Efa6-FL 137 <0.001
H.s. PSD(1)-FL 113 0.003
H.s. PSD2-FL 86 0.001
H.s. PSD3-FL 100 0.001
H.s. PSD4-FL 67 0.25
D
Effects of N-termini on MTs on fibroblast MTs
GFP 116
D.m. Efa6-Nterm 100 <0.001
C.e. Efa6-Nterm 105 <0.001
H.s. PSD(1)-Nterm 113 0.27
E
Effects of putative MTEDs on fibroblast MTs
GFP 116
D.m. Efa6-MTED 45 <0.001
C.e. Efa6-MTED 78 <0.001
H.s. PSD(1)-MTED 98 0.069
F Axon normal
tubulin GFP
F′ Axon damaged
Efa6-GFP
F′′ Axon gone
Efa6-GFP
G MTs normal
tubulin GFP
G′ MTs defect
Efa6-GFP
G′′ MTs gone
Efa6-GFP

Fig. 8 Qu et al.

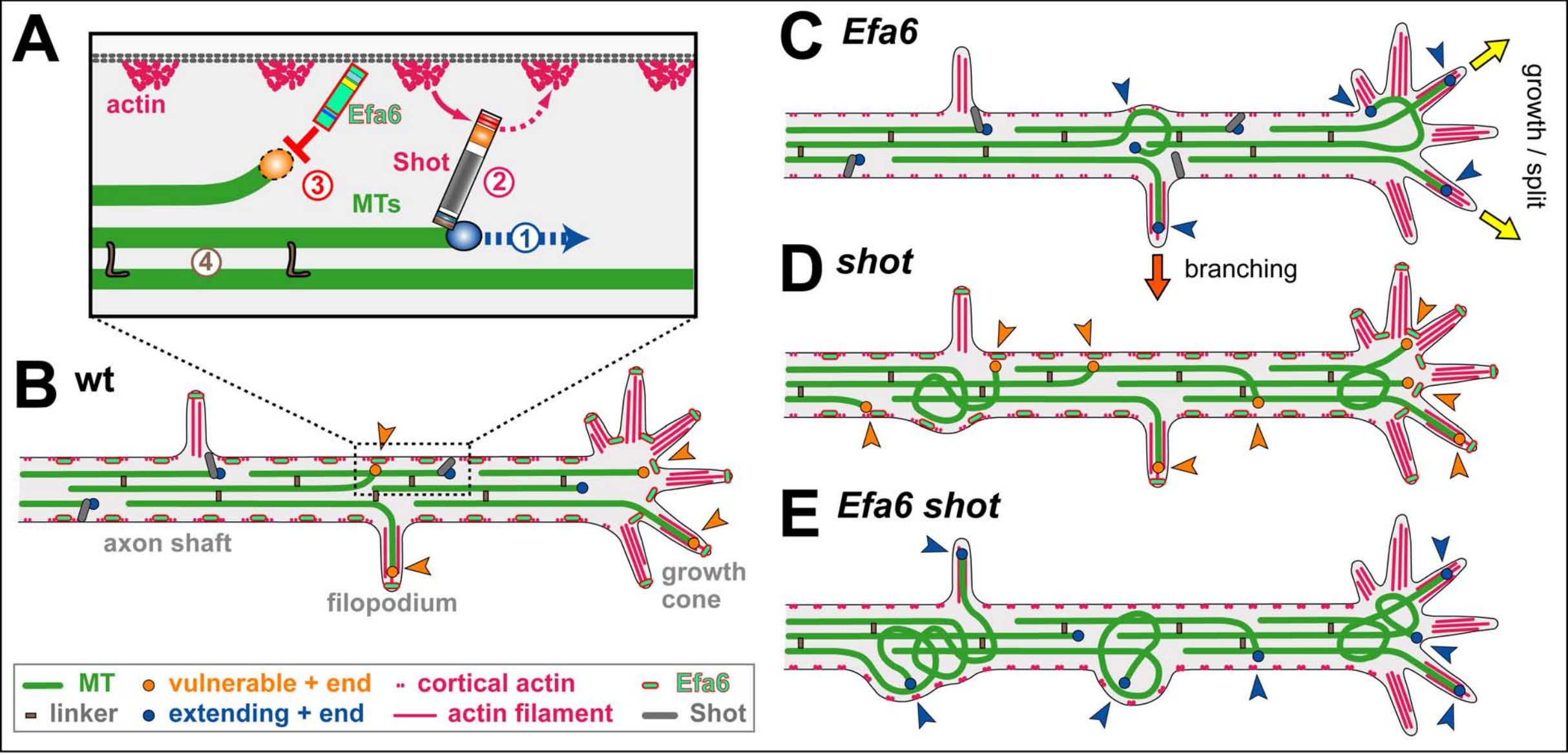
A
actin
Efa6
Shot
MTs
③
②
①
④
B wt
axon shaft
filopodium
growth cone
C Efa6
growth / split
branching
D shot
E Efa6 shot
MT
linker
vulnerable + end
extending + end
cortical actin
actin filament
Efa6
Shot

Fig. 9 Qu et al.

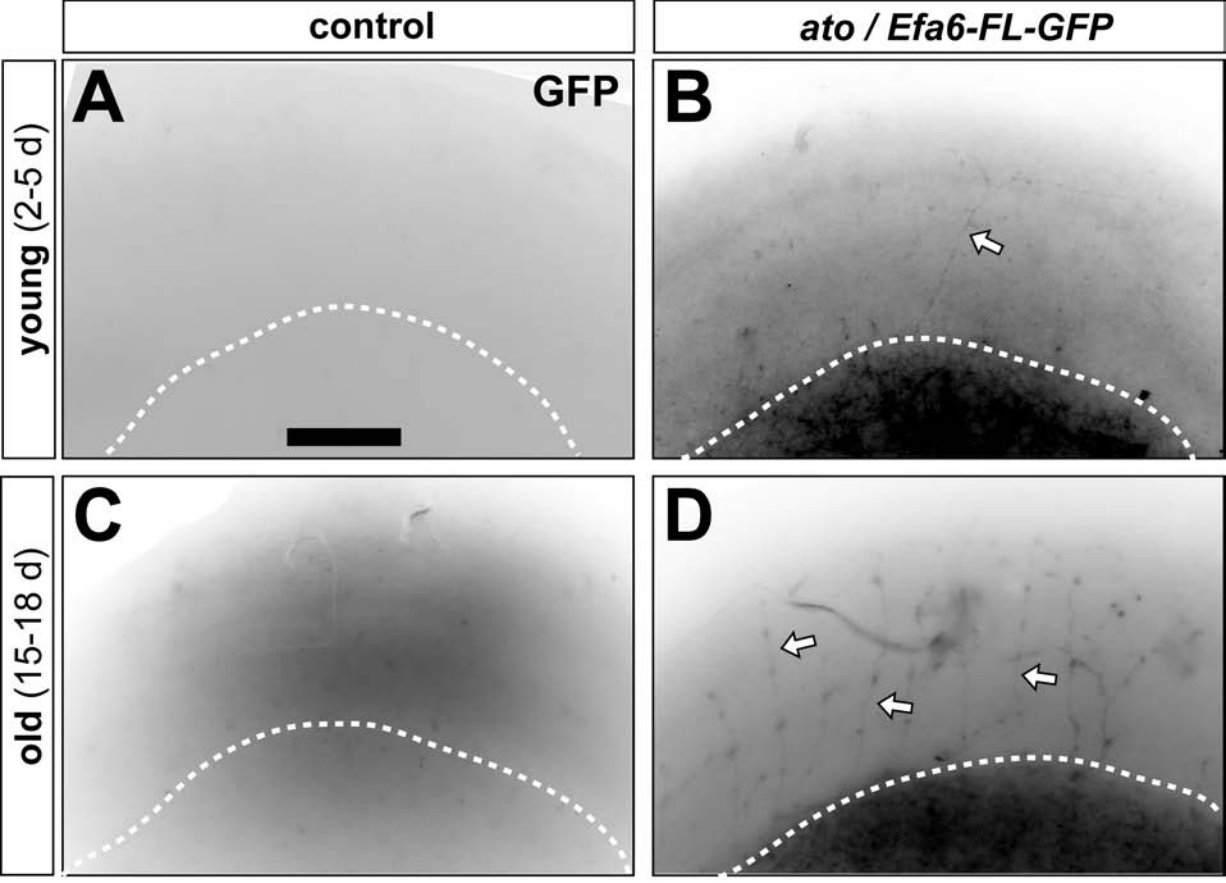

Fig. S1 Qu et al.

MT disorganisation in *Efa6* mutants (binary data)

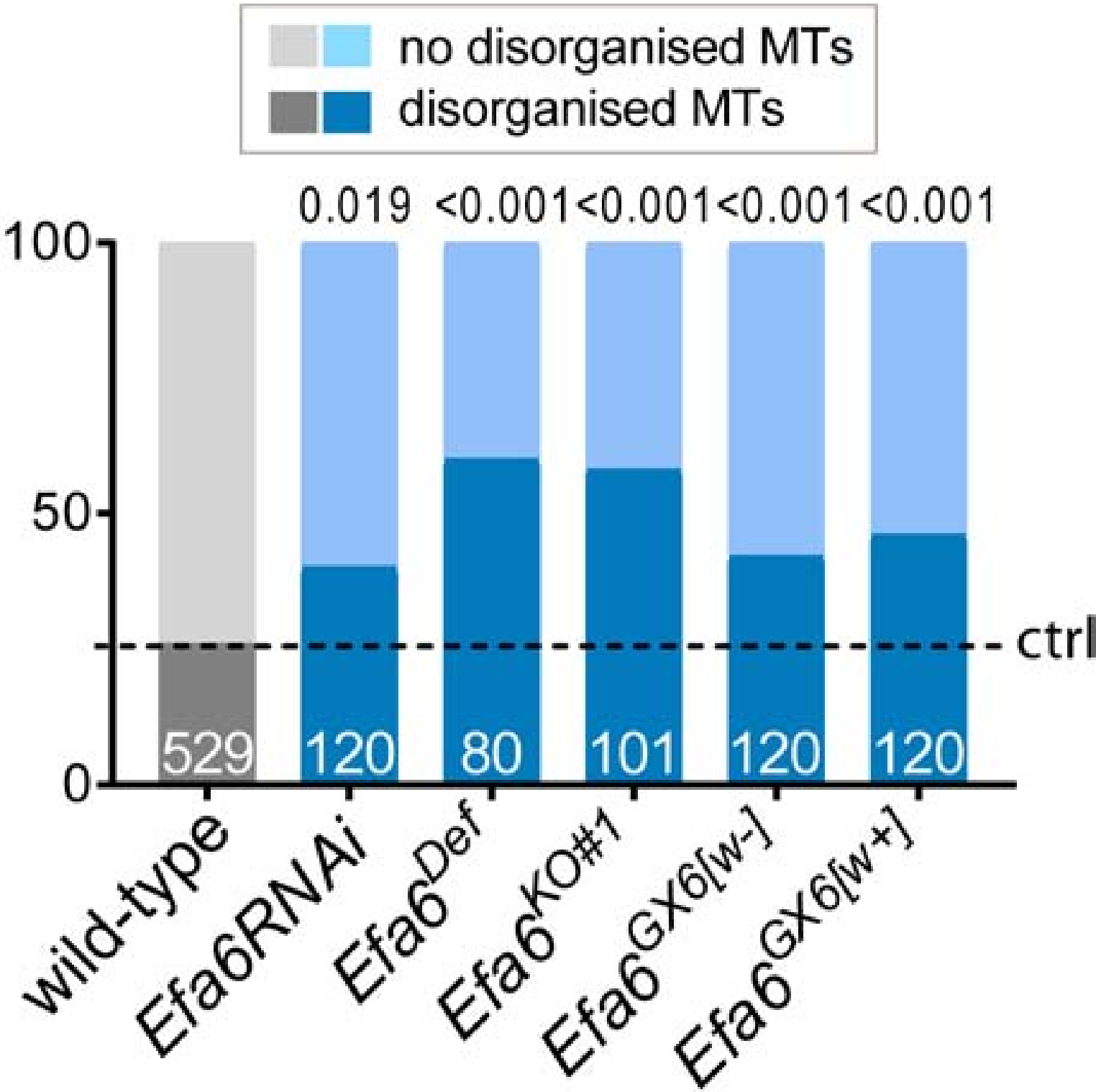

Fig. S2 Qu et al.

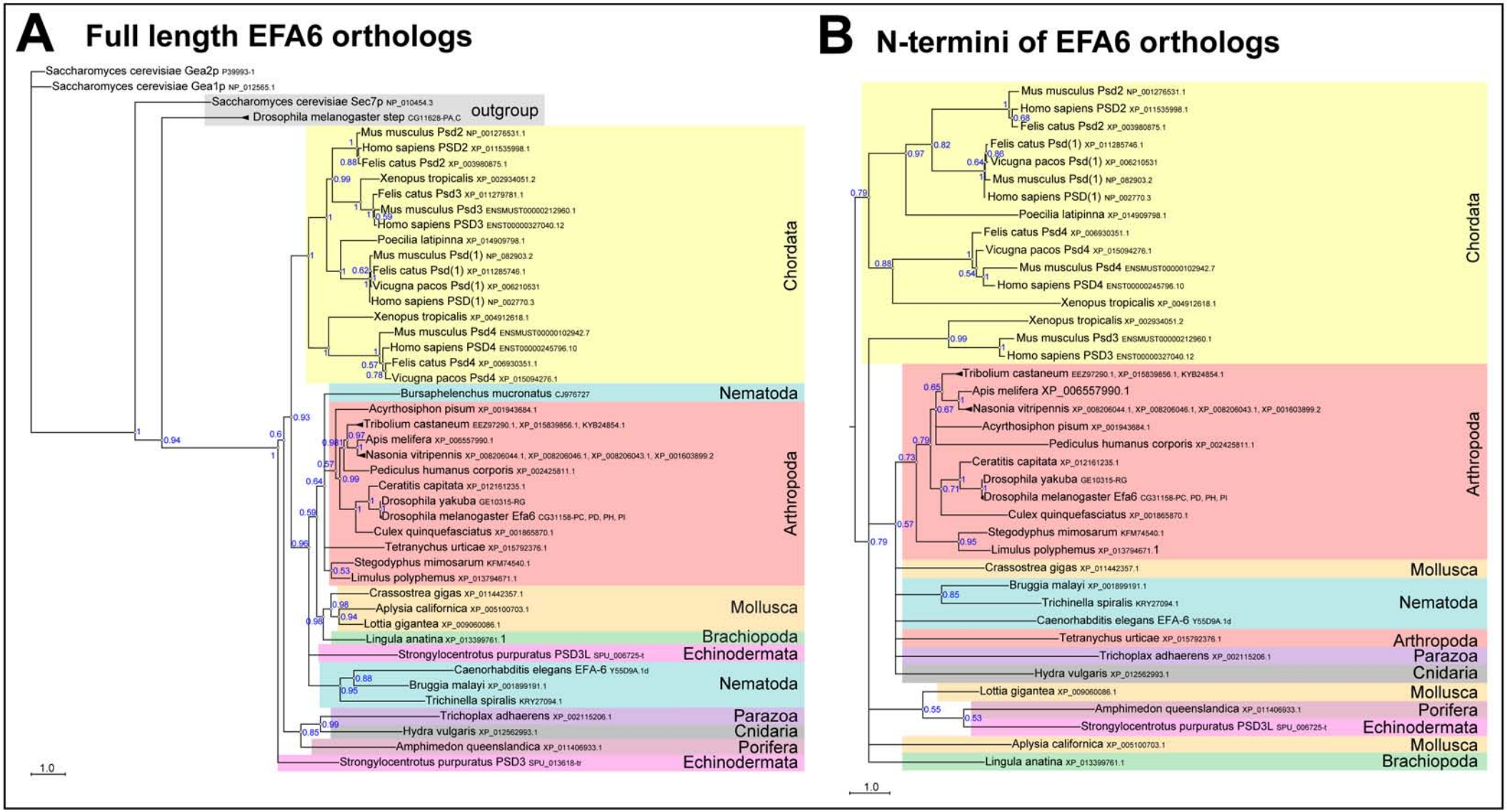

Fig. S3 Qu et al.

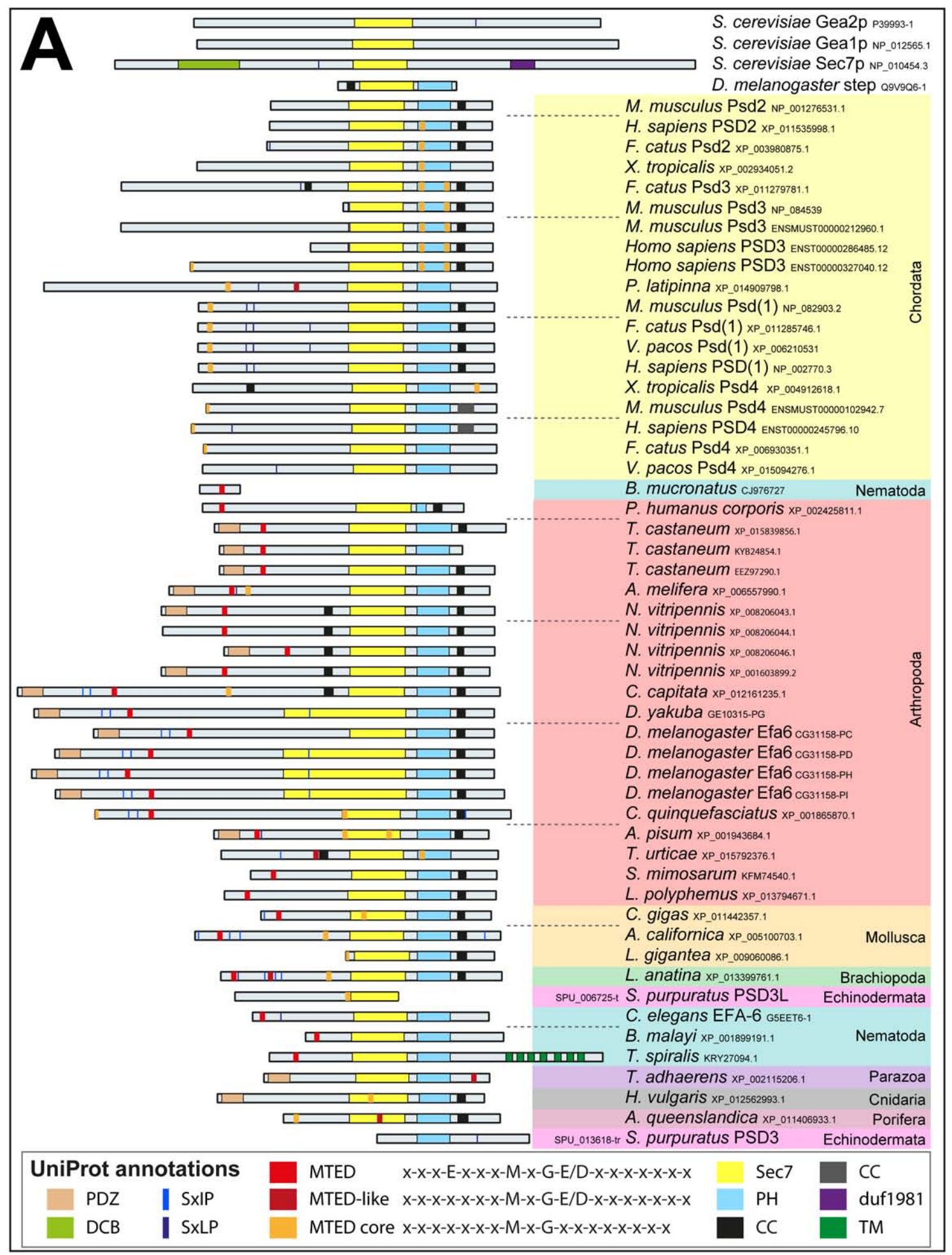

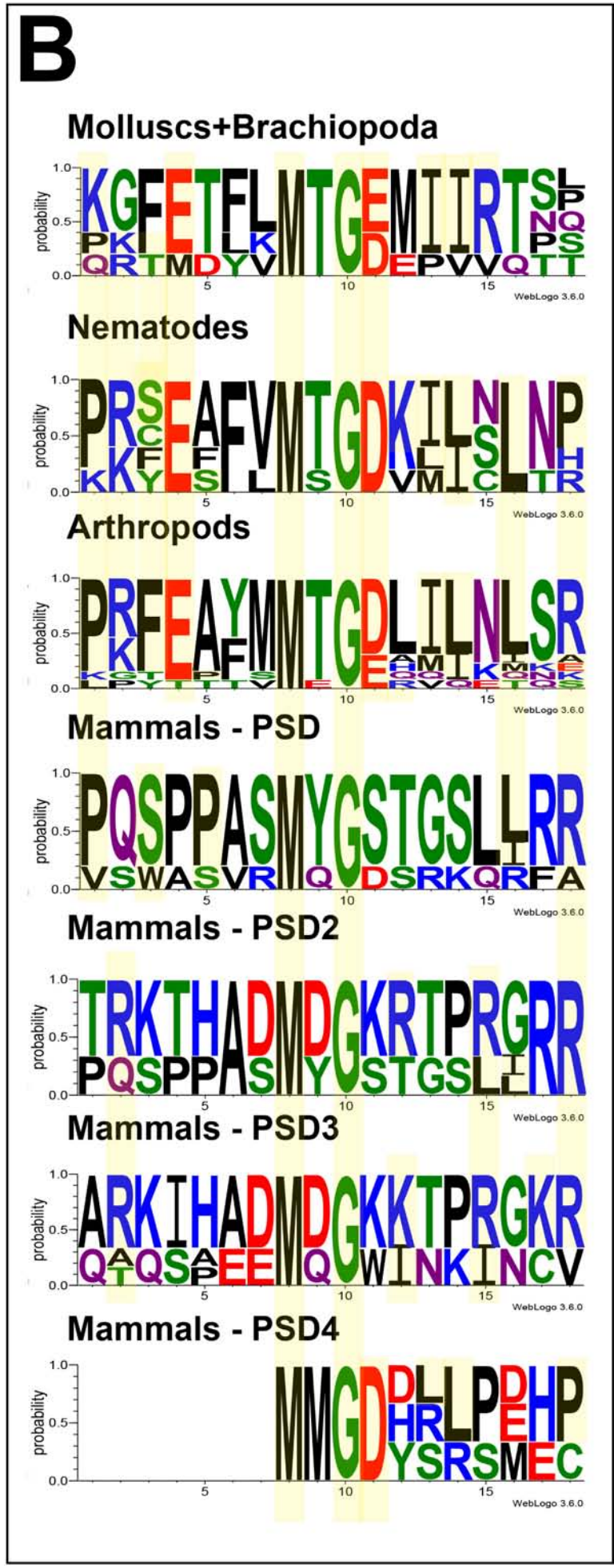

Fig. S4 Qu et al.

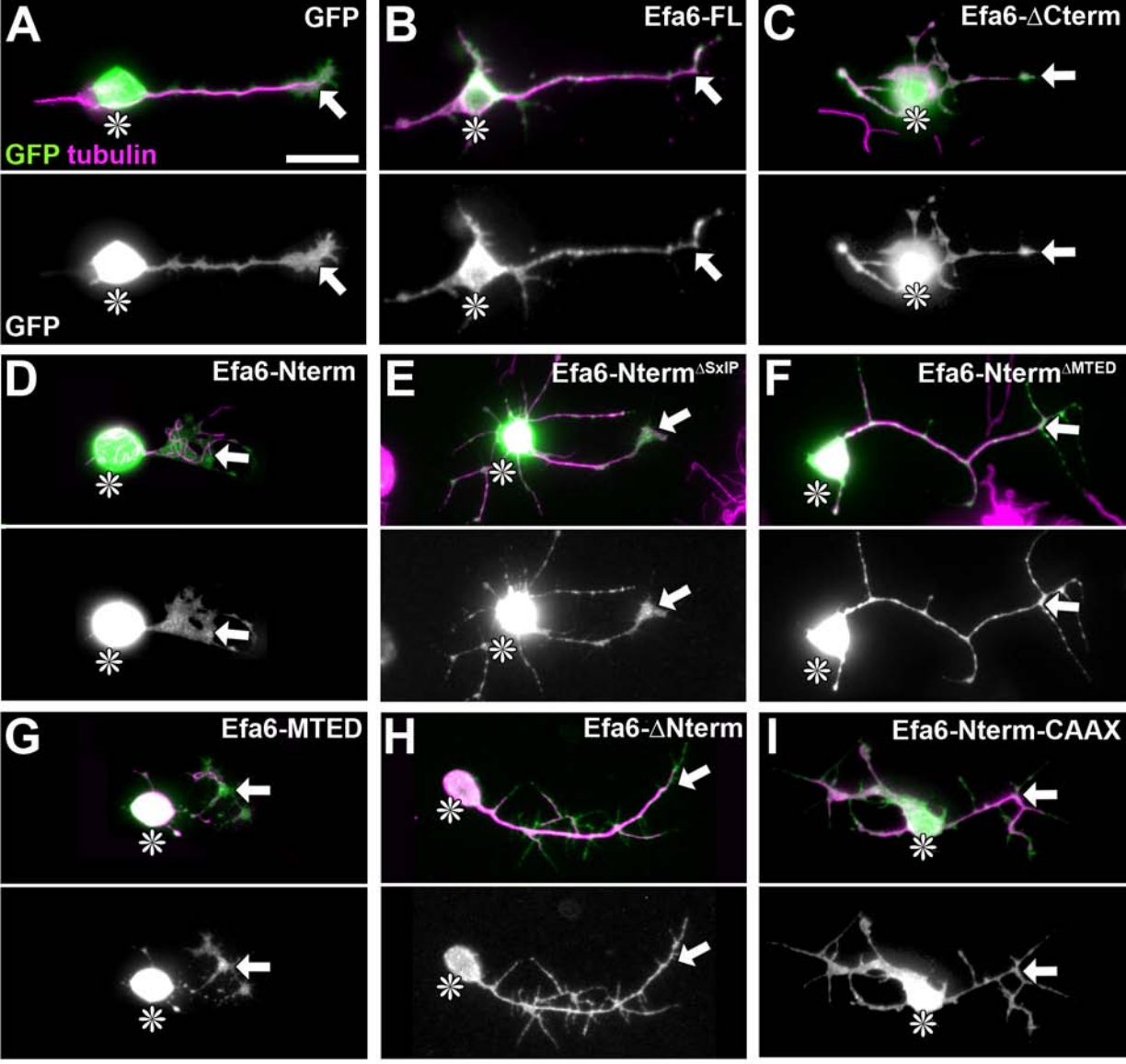

Fig. S5 Qu et al.

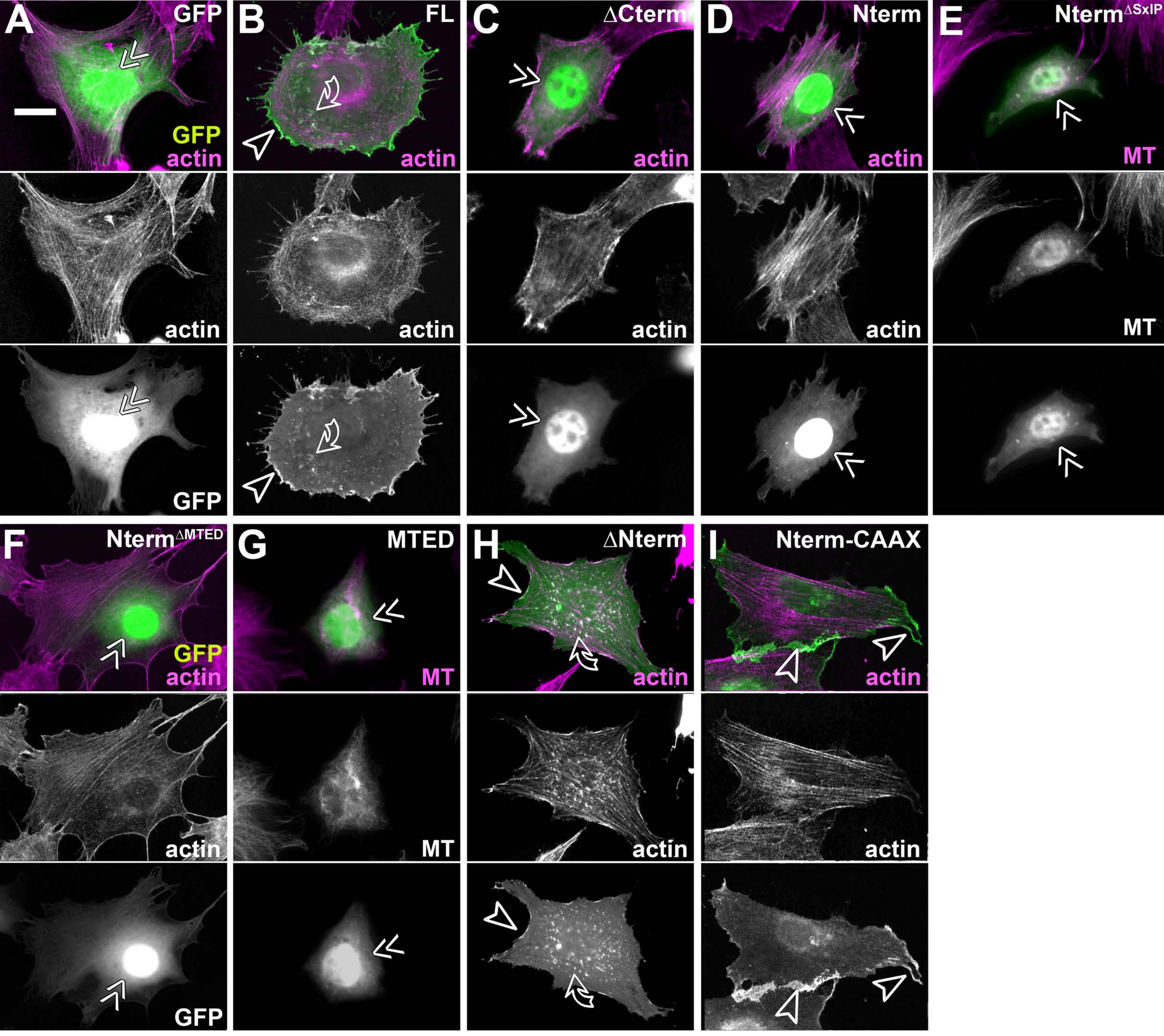

Fig. S6 Qu et al.

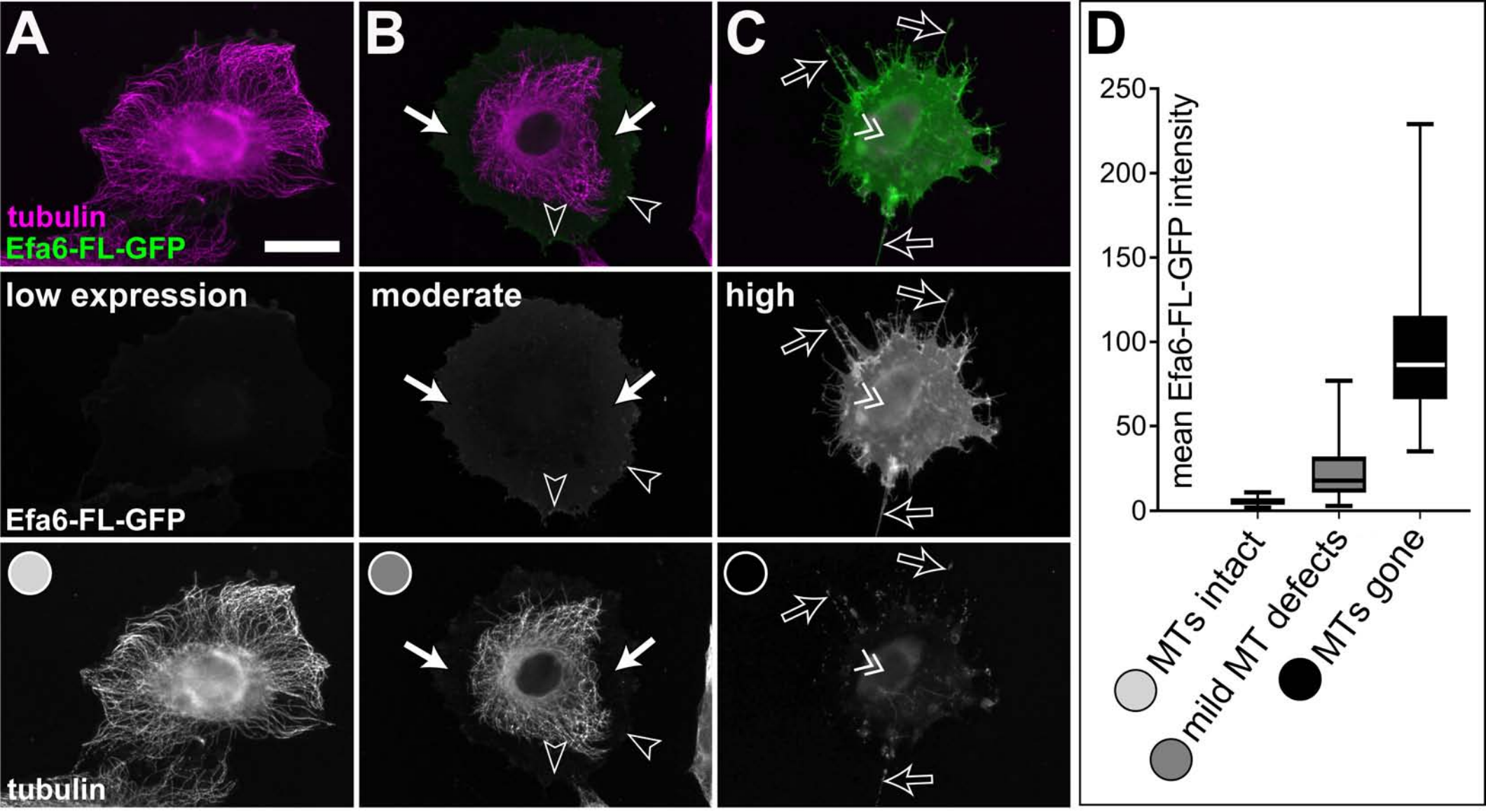

Fig. S7 Qu et al.

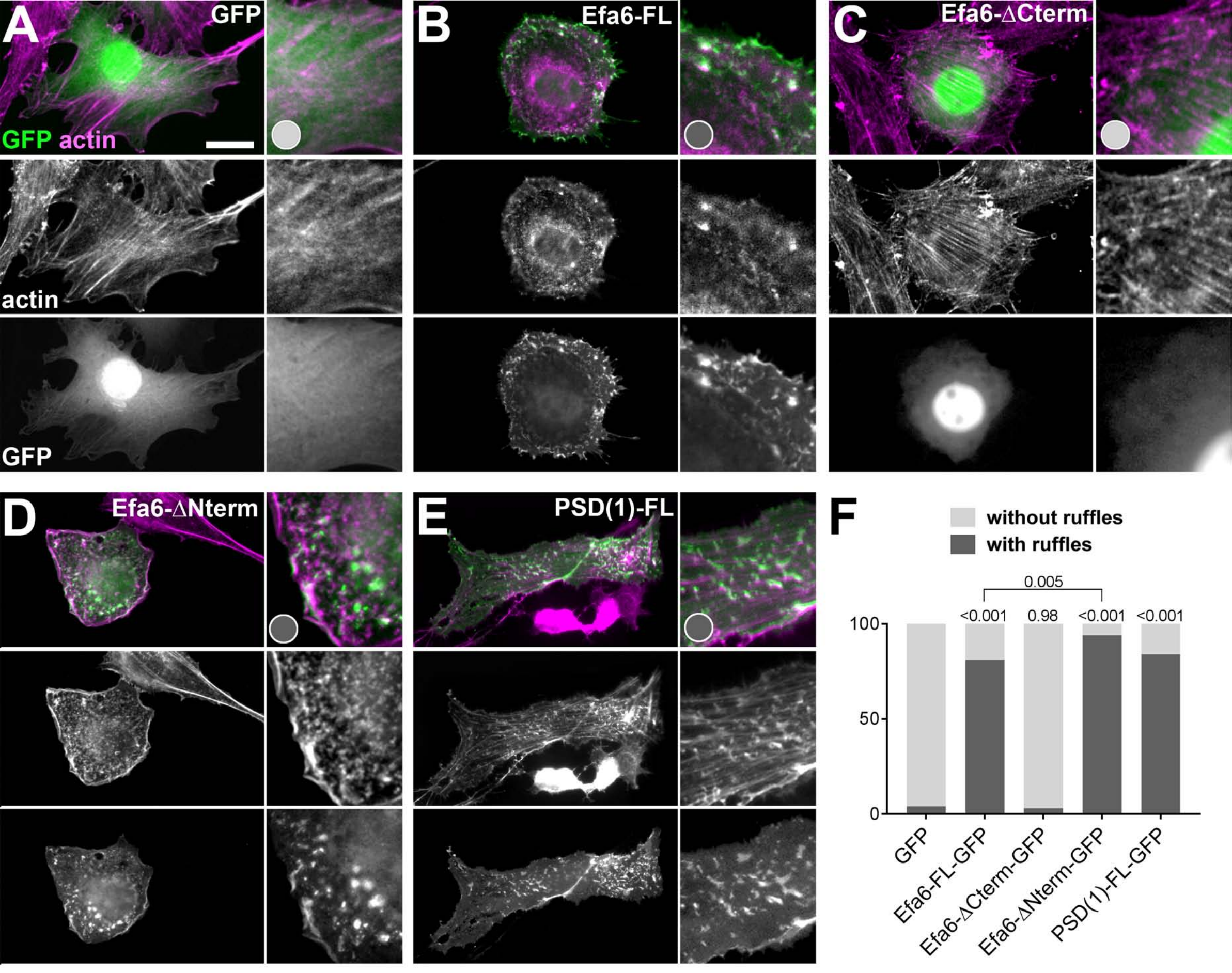

Fig. S8 Qu et al.

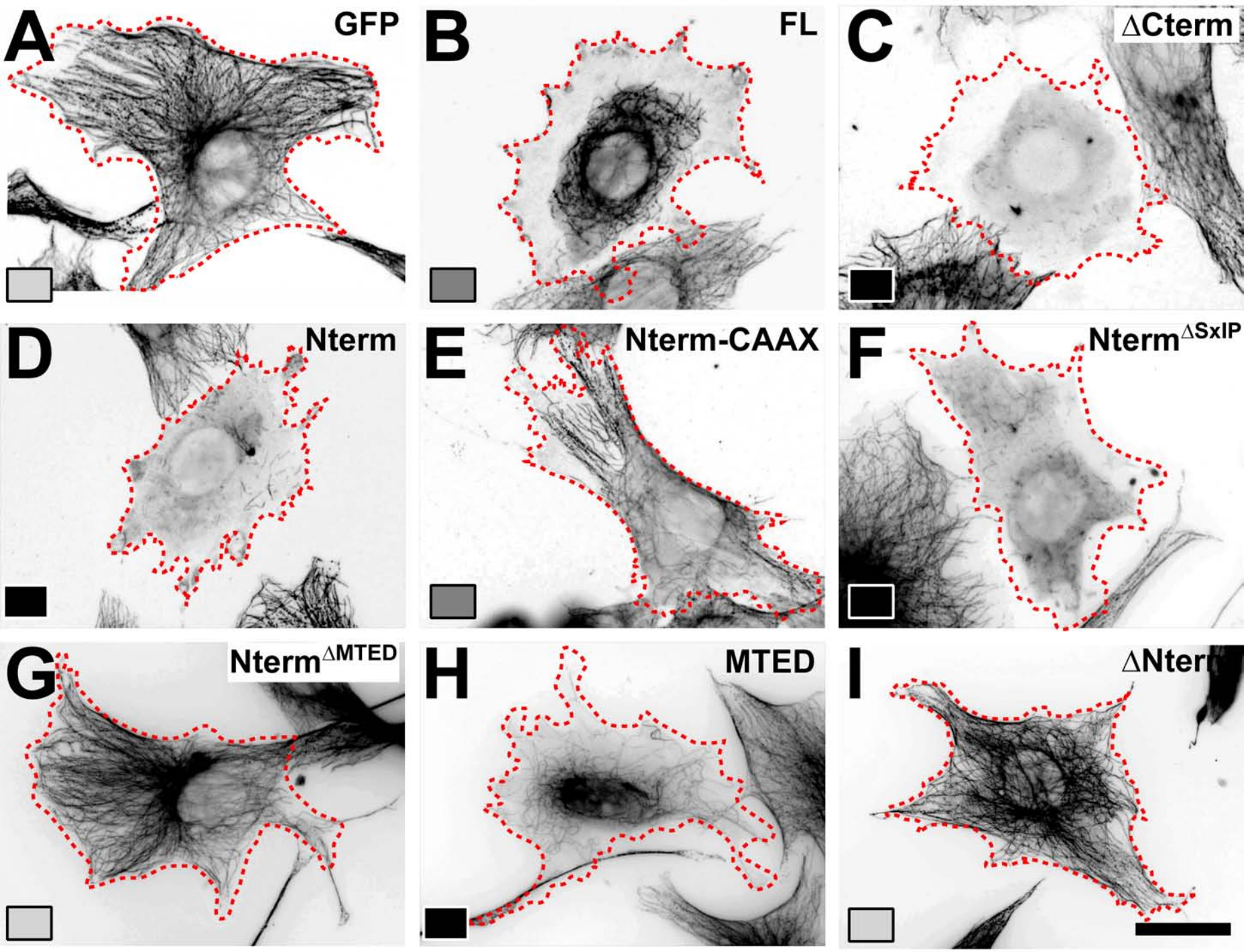

Fig. S9 Qu et al.

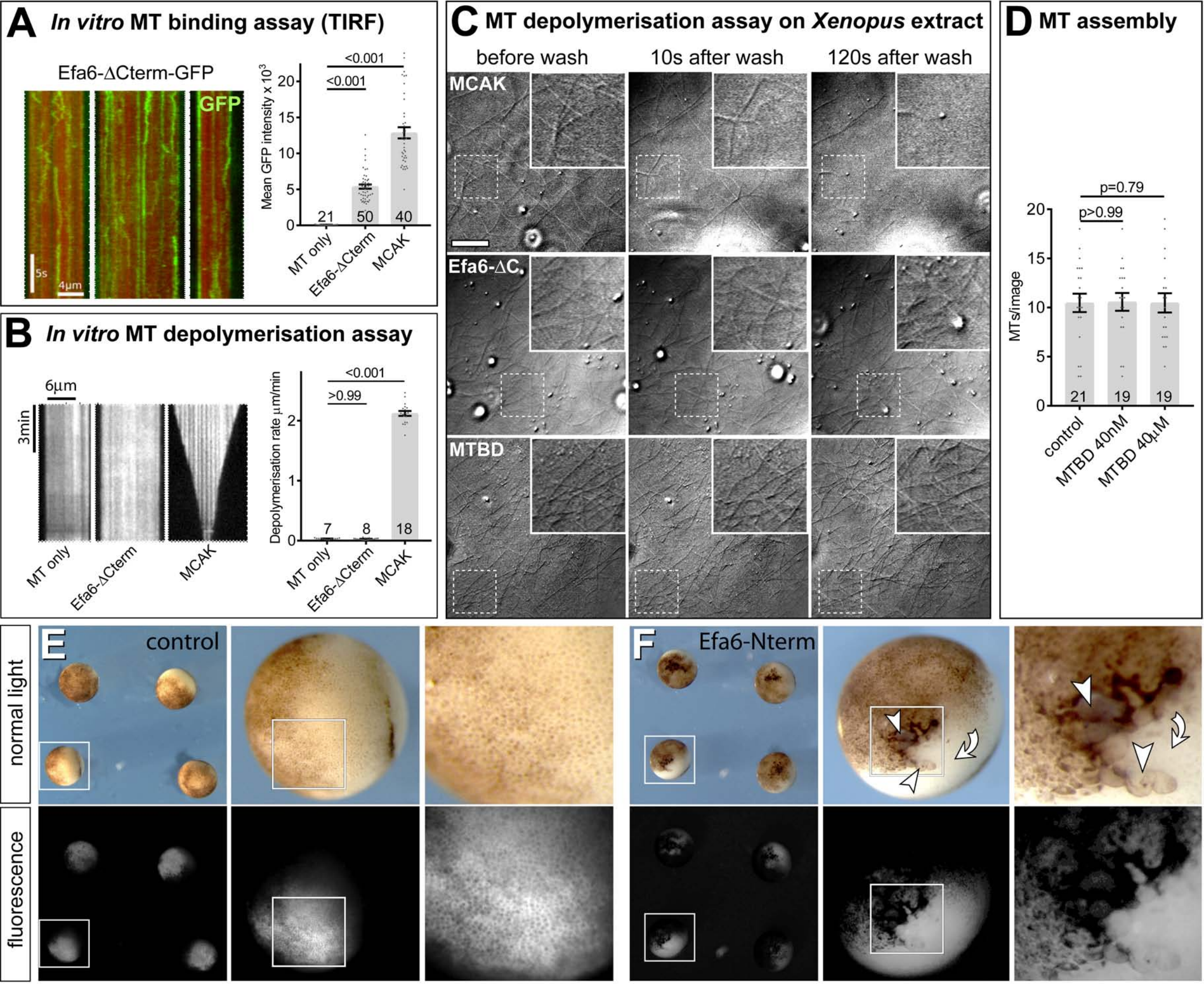

Fig. S10 Qu et al.